Investigating the role of Shroom3 in the mouse cornea

THESIS

Presented in Partial Fulfillment of the Requirements for the Degree Master of Science in the Graduate School of The Ohio State University

By

Elton Angoni, B.S.

Graduate Program in Vision Science

The Ohio State University

2022

Master Thesis Committee:

Timothy F. Plageman, PhD, Advisor

Heather L. Chandler, PhD

Andrew Hartwick, OD, PhD

Copyright by

Elton Angoni

2022

Abstract

Shroom3 is a cytoskeletal protein that is known to trigger the contraction of the cytoskeleton and alter epithelial cell shape. It is comprised of three major domains that are conserved among the Shroom gene family. The SD1 and SD2 domains are well conserved regions among family members and function to localize the protein to cellular junctions, bind actin and Rho-kinase, and induce actomyosin contractile activity. Only the longest isoforms of Shroom3 exons encode a PDZ domain within the translated Shroom proteins. Using whole exome sequencing, a homozygous missense mutation of the *SHROOM3* gene was identified in a patient with keratoconus and hypothesized to be the underlying pathogenetic factor [Tariq et al., 2011]. Furthermore, evidence exists that Shroom3 plays a role in regulating collagen expression. This study is intended to expand our understanding about how *Shroom3* may regulate collagen expression in the cornea. Specifically, it investigates the role of the N-terminal domain found solely in the longest isoform of *Shroom3* and a specific amino acid change within this domain that has been associated with keratoconus.

Methods:

To evaluate the role of the Shroom3 PDZ domain two distinct mouse lines were generated. A homozygous mutation was generated in the mouse Shroom3 coding sequence (G59V) that is homologous to the homozygous polymorphism associated with keratoconus (SHROOM3^{G60V}). The second mouse line was missing a single nucleotide in

an alternative exon that encodes the N-terminal PDZ domain that was predicted to cause a frameshift and premature protein termination (*Shroom3*$^{\Delta iso1}$). Embryonic neuroepithelial tissue collected from *Shroom3*$^{\Delta iso1/\Delta iso1}$ and wild type mice were analyzed by immunofluorescent labeling using Shroom3 and β-catenin antibodies to evaluate the presence of the longest isoform of Shroom3 containing the PDZ domain. Wild type, heterozygous, and homozygous animals of the Δiso1 line were investigated using histological techniques and immunofluorescent imaging. Descriptive statistics including means were used to analyze the collected corneal morphometric measures of features such as corneal thickness. ImageJ was used to evaluate the collected stereomicroscope images.

Results:

Overall assessment of the morphometric corneal features of *Shroom3*^{G59V} line did not uncover any significant differences between wild type (*Shroom3*$^{wt/wt}$), heterozygous (*Shroom3*$^{wt/G59V}$), and homozygous (*Shroom3*$^{G59V/G59V}$) animals. In contrast, the absence of the longest isoform of Shroom3 (*Shroom3*$^{\Delta iso1/\Delta iso1}$) resulted in reduced corneal thickness. Finally, quantitative assessment of collagen expression revealed differences for *Shroom3*$^{\Delta iso1/\Delta iso1}$ mice. Immunofluorescent labeling of type I collagen was decreased in the Δiso1 homozygous mutant when compared with wild type and heterozygous groups. In contrast, type IV collagen was ectopically expressed in the mutant corneas.

Conclusion:

The study suggests that the longest isoform of Shroom3 which contains an N-terminal PDZ domain is necessary for maintaining corneal thickness and regulating collagen expression.

Dedication

This document is dedicated to my family.

Thank you for the immense support, always showing interest for my research project, and believing in my abilities. Your encouragement and your presence are precious to me!

Acknowledgments

First and foremost, I would like to give my thanks to my research supervisor; Thank you Dr. Timothy Plageman for the trust you have granted me and for the wisdom you have imparted at the start of my T35 internship in the summer of 2019. It is without a doubt that this first opportunity in research propelled my desire to pursue a master's degree. I would also like to sincerely thank him for his constant support and his presence throughout my master's degree. His encouragement, his detailed explanations and carefully crafted ideas certainly contributed to the success of my research project. I am incredibly grateful for his guidance throughout my research during such a tumultuous time.

Also, I would like to thank the research staff at the lab; Ken Herman, Nathalie Houssin and Jessica Martin for the support and guidance they offered me. The detailed instructions they provided in the proper maintenance and application of laboratory procedures simplified and improved my time doing research. It is thanks to them that I managed to carry out my research project independently. I want to specifically give a big thank you to Jessica Martin, as it due to her patient guidance that I was able to navigate and organize my first few experiments. I would also like to thank Jessica Herstine and the other students working at the lab who made research a much more enjoyable experience. Your collaboration with my research project is very dear to me.

And finally, I would also like to thank the Graduate School of The Ohio State University and my thesis committee: Dr. Chandler and Dr. Hartwick. Thank you for taking the time to review my thesis your feedback and expertise is greatly appreciated.

Vita

May 2015 .....Arts and Sciences, Marianopolis College

2018.....B.S. Biology, McGill University

Fields of Study

Major Field: Vision Science

Table of Contents

List of Tables

List of Figures

Chapter 1: Introduction

Cellular and histological structure of the cornea

The cornea is the curved, transparent, and outermost ocular tissue that plays a crucial role for vision as the main refractive component of the visual system to focus images onto the retina [Trattler et al., 2010; Henriksson et al., 2012; Bergmanson & Doughty, 2005]. This ocular tissue is composed of five histologically distinct layers that include the epithelium, Bowman's Layer, the stroma, Descemet's membrane, and the endothelium [Smith et al., 2002; Henriksson et al., 2009]. It is bordered anteriorly by a tear film and posteriorly by the aqueous humor. To maintain the cornea's transparency and refractive properties, its largest layer, called the stroma, must maintain highly regularly sized and organized collagen fibrils [Henriksson et al., 2009; Quantock et al., 2015; Chen et al., 2015]. Disruption in the structural organization of any of the corneal layers due to pathologies can threaten vision [Shetty et al., 2015; Eghrari et al., 2015]. It is therefore imperative to investigate the etiology of these changes within the cornea.

Elucidating the changes that occur within pathological corneas require an understanding of the anatomy and physiology of a healthy cornea. An important function of the cornea is to provide a barrier that protects the eye from external agents. Its outermost layer, the epithelium, serves to shield the eye from pathogens and additional environmental hazards. Environmental pathogens are shielded from the ocular surface via a transmembrane mucosal barrier called the glycocalyx formed from the mucin secretions of corneal epithelial cells [Mantelli, 2013]. The glycocalyx acts as a barrier to polarized

molecules and cannot freely access the ocular surface due to the electrochemical nature of mucins. This protective function is further aided by tight junctions located between cells and create an intercellular barrier that prevents and/or limits the paracellular transport of environmental pathogens [Yi et al., 2000].

The basement membrane of the epithelial layer is mainly composed of laminins, collagen, proteoglycans, and nidogen [Torricelli et al., 2013; Wilson, 2020]. It serves as a physical link between the basal side of the epithelial layer to the more posterior Bowman membrane. The basal portion of epithelial cells are anchored to the basement membrane via protein complexes called hemidesmosomes [Wilson, 2020; Kabosova et al., 2007]. These molecular structures are tightly attached to both the underlying basement membrane and to Bowman's layer through anchoring filaments and anchoring fibrils. While the basement membrane filaments are composed of laminin and collagen IV [Wilson, 2020], the anchoring fibrils of Bowman's layer are composed of type VII collagen [Eghrari et al., 2015; Torricelli et al., 2013]. Bowman's layer is acellular and is formed by randomly arranged type I collagen in addition to some forms of types V, VII, and XII collagens; type XII collagen being that which provides the structural stability to this layer [Wilson et al., 2020]. Any disruption that perturbs the connection of the epithelium with Bowman's layer can result in various pathologies, including a group of disorders known as superficial corneal dystrophy. It is thought that these pathologies are mostly linked to gene mutation rather than inflammation [Klintworth, 2009].

The corneal stroma (Figure 1A), which lies between Bowman's layer and Descemet's membrane, constitutes nearly 90% of the corneal thickness [Meek & Koupp,

2015; Henriksson et al., 2009]. This layer is composed of collagen proteins in triple helical structures that interconnect to form collagen fibrils. Multiple parallel collagen fibrils are tightly packed and organized afterwards into lamellae [Meek & Knupp, 2015]. Their dimension in humans can range up to 0.2 mm broad and 2μm thick [Komai & Ushiki, 1991]. Lamellae have variable thicknesses and in humans, the center cornea holds nearly 200-250 lamellae layers, with a higher density within the anterior stroma when compared to posterior stroma [Bergmanson & Doughty, 2005]. The anterior stroma of a normal cornea contained collagen lamellae which are narrow, highly interlaced [Radner et al., 1998], and randomly orientated [Komai & Ushiki, 1991], with most appearing to insert into Bowman's layer [Morishige et al., 2006; Henriksson et al., 2012]. Radner et al. has shown that the lamellae in the mid-stroma are also highly interlaced [Radner & Mallinger, 2002], whereas they are less interwoven and more structurally oriented in the posterior stroma [Radner & Mallinger, 2002; Meek et al., 1987]. The spatial arrangement of the collagen fibrils and their organization into lamellae within the stroma offers transparency and biomechanical strength [Meek & Knupp, 2015].

Type I collagen is the most abundant form of collagen in the human body and along with collagen type V are major constituents of the corneal stroma in multiple species [Myllyharju & Kivirikko, 2004; Henriksson et al., 2009]. During corneal collagen fibril deposition, a procollagen molecule is produced that consists of three individual proteins, two pro-α1 chains and one pro-α2 chain, which are expressed from the COL1A1 and COL1A2 genes, respectively [Ricard-Blum, 2011]. Corneal collagen type I arranges itself and attaches to collagen type V to form long, thin fibrils. The mixture of collagen I and V,

known as fibrils, then link to one another to form strong collagen lamellae [Ricard-Blum, 2011]. Interrupting the organization of the fibrils within the cornea deteriorates its ability to maintain corneal transparency, leading to a reduction in visual acuity.

The cells responsible for producing and maintaining collagen structure within the stroma are called keratocytes and are located between lamellae. [Lwigale et al., 2005]. Keratocytes produce collagen molecules and proteoglycans. These cells also secrete matrix metalloproteinases to facilitate protein turnover [Young et al., 2009]. Stromal extracellular matrix secreted by keratocytes is composed of various types of proteoglycans. Keratan sulfate proteoglycans in the stroma include luminican, keratocan and mimecan [Torricelli & Wilson, 2014, Eghrari et al., 2015].

Disruptions to this highly organized structure can result in an opaque cornea, [Kostyuk et al., 2002; Regini et al., 2004; Meek & Knupp, 2015] thus reducing vision. The diameter and spacing of collagen fibrils within the corneal stroma are strictly maintained [Maurice et al., 1957]. The uniform spacing is due to the presence of interfibrillar and highly negatively charged proteoglycans. By binding to collagen fibrils, they modulate interfibrillar spacing by repelling other highly charged neighboring fibrils [Kao & Liu, 2002; Meek & Knupp, 2015]. The uniform diameters of the collagen fibrils and precise spacing in the cornea allows for light to propagate forward without scattering [Meek & Knupp, 2015]. This molecular architecture promotes corneal transparency and is paramount for vision [Carlson et al., 2003; Meek & Knupp, 2005; Henriksson et al., 2012]. Thus, when collagen fibril organization is disrupted corneal pathologies, such as keratoconus, reduced vision can occur.

The most posterior part of the cornea is the endothelium. It consists of a monolayer of regular polygonal cells and is involved in corneal transparency by simultaneously providing a barrier as well as ion, water, and metabolite transport functions [Srinivas, 2010]. The endothelium's sodium potassium pumps osmotically draw water and ions from the stroma into the aqueous humor aiding the maintenance of corneal transparency [Feizi, 2018]. Additionally, the endothelium produces Descemet's membrane. Descemet's membrane is an acellular layer located between the endothelial layer and the stroma. In contrast to the stroma, it contains type IV collagen. Type IV collagen contains three identical α-I Type IV polypeptide chains which differ from other α-chains [Lodish et al., 2000]. The proper maintenance and regulation of each corneal layer is integral in the cornea's ability to remain transparent and offer visual clarity; the obstruction of that maintenance in diseases like keratoconus can lead to devastating functional outcomes for the patients involved.

Keratoconus is a multifactorial vision disorder with unknown etiology

Keratoconus is a non-inflammatory, typically bilateral dystrophy of the cornea [Wagner et al., 2007; Dudakova et al., 2014] and is the most common corneal ectasia disorder in developed countries [Kim et al., 1999; Gomes et al., 2015]. Corneal ectasia is defined as the bulging of the cornea (Figure 1B) leading to a conical shape and visual distortion [Greenstein & Hersh, 2021]. These physical changes occur because of corneal thinning and overall alterations to the cornea's structure and organization [Shetty et al., 2015; Ehgrari et al., 2015]. Disintegration of the epithelial basement membrane, scarring

at both the level of the Bowman's membrane and the stroma, as well as keratocyte modification are also aspects of this pathology [Martínez-Abad & Piñero, 2017; Gustafsson et al., 2020]. Its estimated incidence varies from 2 to 50 per 100,000 in the general population and prevalence from 10 to 55 per 100,000 [Kennedy et al., 1986; Rabinowitz, 1998; Mohammadpour et al., 2017]. The disparity in estimated incidence is partly due to the different diagnostic criteria used in various studies [Ihalainen, 1986; Hashemi et al., 2020]. Typically, this disorder begins at puberty and progresses slowly over time. In its early forms, keratoconus can be detected and quantified with corneal topography, a three-dimensional procedure that maps the anterior and sometimes posterior surface of the cornea by capturing projected reflected beams of light [Rabinowitz, 1998]. As the disease progresses, patients require frequent adjustment to their visual correction and eventually, visual acuity cannot be properly corrected using spectacles [Gommes et al., 2015]. Other non-surgical treatment options, such as rigid gas-permeable contact lenses, may also reach a point when they are unable to correct or prevent visual reduction in more severe cases of this disorder. In patients with an advanced form of keratoconus, treatments include either a deep anterior lamellar keratoplasty or penetrating keratoplasty. Deep anterior keratoplasty is a surgical procedure that removes the corneal stroma and Descemet's membrane, replacing it with healthy donor corneal tissue [Ionescu et al., 2016]. A full-thickness cornea transplant, or what is known as penetrating keratoplasty, is used in advanced stages of keratoconus when the integrity of the corneal epithelium or Descemet's membrane is altered beyond repair. About 15 to 60% of keratoconus patients undergo penetrating keratoplasty [Rebenitsch et al., 2011; Akhtar et al., 2013]. In 2019, keratoconus

was the sixth most common specific indication for transplants performed in the United States [2019-EBAA-Stat-Report]. These data suggest that keratoconus is a public health burden due to the negative impact on the involved individuals' quality of life as they experience a continuing decline in their vision [Rebenitsch et al., 2011]. Further investigation into the etiology of keratoconus is a crucial endeavor that is necessary to identify and target treatments for individuals at risk.

Keratoconus is associated with structural changes in the organization of collagen within the cornea that are present at different stages of the disease. One observed change is a significant reduction in the number of lamellae [Morishige et al., 2007], particularly in the anterior and posterior stromal layers [Mocan et al., 2008; Erie et al., 2002; Sykakis et al., 2012], causing overall thinning of the cornea. Another change is the splitting of stromal lamellae into multiple bundles of collagen fibrils that eventually leads to the loss of anterior lamellae [Mathew et al., 2015]. A reduced number of lamellae and loss of cohesion between collagen fibrils and the non-collagenous matrix allows inter-lamellar slippage to occur within the stroma [Daxer & Fratzl, 1997; Smolek & Beekhuis, 1997; Fullwood et al., 1992]. As the structure of the stromal lamellae changes, it is then followed by the uneven dispersion of the collagen fibrillary mass, particularly around the center of the bulge [Meek & Boote, 2009]. Mechanistically, keratoconus is thought to be the result of the reduced mass of the stromal collagen and the slippage within collagen lamellae [Meek et al., 2005]. Additional changes seen in keratoconus, include a reduction in keratocyte number due to increased cell apoptosis and lower levels of proliferation [Song et al., 2015; Kaldawy et

al., 2002; Kim et al., 1999]. Although it is unclear how or why these changes occur, it is well supported that stromal integrity is destabilized in keratoconus.

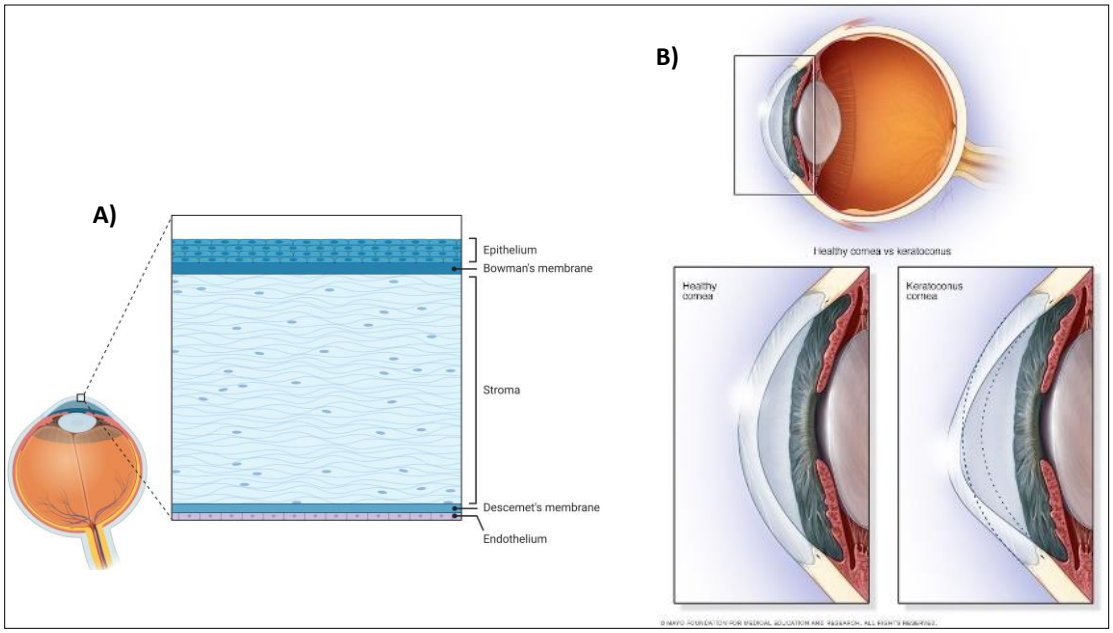

Figure 1. Corneal anatomy and Keratoconus. A) The diagram depicts layers of a normal cornea (CreateBioRender.com); B) Keratoconus is an eye disorder that occurs when the cornea thins and gradually bulges outwards into a cone shape (Mayo Foundation).

Although the etiology and pathogenesis of keratoconus remains poorly understood [Gordon-Shaag et al., 2015; Davidson et al., 2017], genetic, metabolic, immunological, and ecological factors have all been suggested [Gomes et al., 2015; McMonnies, 2005; Wheeler et al., 2012; Gordon-Shaag et al., 2015]. Individuals who have a positive family history of the corneal ectasia are recognized to be at increased risk in developing keratoconus, suggesting a genetic predisposition may exist [Wheeler et al., 2012]. Among familial cases,

the pattern of inheritance is most commonly autosomal dominant [Rabinowitz et al., 1992] and monozygotic twins are often concurrently afflicted with keratoconus. Environmental elements, such as contact lens wear, eye rubbing, and atopy of the eye [Krachmer et al., 1984; Rabinowitz, 1998, Sugar & Macsai, 2012] are all possible contributing factors to the development of keratoconus, especially in individuals with a family history [Gordon-Shaag et al., 2015].

Next generation sequencing, whole genome and exome sequencing have all been utilized in various studies to identify genes directly linked to keratoconus [Rabinowitz et al., 2021]. A mutation of the miR184 gene, a non-coding RNA that regulates gene expression, is linked to keratoconus, and thought to play a role in the disease's etiology [Hughes et al., 2011]. MicroRNAs are part of the RNA-silencing complexes and play an active role as post-transcriptional regulators and can effectively reduce protein expression. In the eye, miR184 is found mostly in the basal cornea epithelial cells and lens and mutations in this gene are thought to disrupt gene regulation of key proteins such as ITGB4 that required to preserve corneal tissues and prevent apoptosis [Ryan et al., 2006,]. g [Hughes et al., 2011]. Missense mutations in the *DOCK9* gene are also associated with keratoconus [Czugala et al., 2012]. This change is located within its DHR1 domain which is a highly conserved region that is involved with protein-protein interaction and recruitment to cellular membranes. Single nucleotide polymorphisms (SNPs) of additional genes associated with keratoconus have been identified using genome-wide association studies that predict disease association by correlating it with specific genetic variations. [Khawaja et al., 2019]. Interestingly, one example study identified SNPs within the genes

FOXO1, *ZNF469*, and *FNDC3B* that were correlated with a decrease in corneal hysteresis, corneal resistance, and corneal thickness and suggests a possible etiology for keratoconus [Khawaja et al., 2019]. The ability of *FOXO1* to regulate collagen expression may also contribute [Tanaka et al., 2009]. Despite research supporting a genetic component in the development of keratoconus, how these SNPs alter gene function to cause disease is poorly understood.

SHROOM3 function and link to keratoconus

Among the genes associated with keratoconus is *SHROOM3* (Figure 2A). Using whole exome sequencing, a homozygous missense mutation in *SHROOM3* was identified and hypothesized to be the cause of cardiac heterotaxy and keratoconus in a human subject [Tariq et al., 2011]. The homozygous mutation changed a glycine codon (GGG) to a valine codon at amino acid position 60 (G60V), which is highly conserved in the Shroom3 protein across species (Figure 2E) [Tariq et al., 2011]. Furthermore, a single nucleotide polymorphism in the *SHROOM3* gene near the PSD-95/Dgl/ZO-1 (PDZ) domain has been associated with alterations in central corneal thickness [Dimasi et al., 2010]. It is therefore possible that the Shroom3 protein plays a mechanistic role in the maintenance of corneal structure.

Shroom3 is among a small family of actin-binding proteins (Shroom 1-4) that play an important role in organizing the actin cytoskeleton [Hagens et al., 2006]. Shroom3 is required for several developmental processes through its role in shaping the morphogenesis of epithelial tissues [Farber et al., 2011; Hildebrand and Soriano, 1999; Plageman et al.,

2011a; Plageman et al., 2011b; Nishimura & Takeichi, 2008]. The function of Shroom3 is exerted through its binding to Rho-kinase (ROCK) and consequently the activation of ROCK-myosin II pathway that triggers the contraction of apical junction localized actin filaments [Hildebrand and Soriano, 1999; Hildebrand, 2005]. Most of what is understood about Shroom3 function has been in the context of epithelial tissues and not mesenchymal tissues such as the stroma.

The Shroom family of proteins are characterized by the presence of three distinct and highly conserved domains (Figure 2B, 2C) [Lee et al., 2009]. The SD1 and SD2 domains are required for the majority of the known functions of Shroom proteins. The SD1 domain, is somewhat centrally positioned and binds directly to F-actin and facilitates Shroom3 localization to the cellular junctions [Hildebrand and Soriano, 1999; Grosse et al., 2011). The SD2 domain is required for Rho-kinase binding and Shroom3-mediated contractile activity [Hildebrand and Soriano, 1999; Dietz et al., 2006]. An N-terminal PDZ domain is also present. PDZ domains are recognized to play a role in intracellular signaling events and mediating protein-protein interactions [Ponting et al., 1997; Jemth & Gianni, 2007]. Shroom3 has two isoforms, the longest isoform has the PDZ domain, and the shortest isoform does not (Figure 2C). While the function of the PDZ domain is not known the ability of Shroom3 to modify the cytoskeleton is independent of it. The shortest isoform, which lacks this domain is sufficient to induce apical constriction [Hildebrand, 2005].

A newly discovered function of Shroom3 appears to be the regulation of collagen expression. This was revealed through the analysis of patients with chronic kidney disease

that are associated with a single short nucleotide polymorphism (SNP) within the SHROOM3 gene [Köttgen et al., 2009; Böger et al., 2011; Deshmukh et al., 2013]. This SNP alters an intron within the SHROOM3 gene and causes an increase in its expression. Additional analysis indicated that Shroom3 positively regulates the fibrosis program that includes the upregulation of collagen expression in kidney tissue [Menon et al., 2015]. Thus, the upregulation of Shroom3 in the kidneys of these patients are hypothesized to cause kidney fibrosis and alter collagen expression [Menon et al., 2015]. An investigation into the role of Shroom3 in mouse corneal development and collagen regulation was also carried out. [Lappin, 2018]. These results showed that in embryos lacking Shroom3 corneal tissues exhibited a reduced number of keratocytes and an increase in collagen fibril diameter [Lappin, 2018]. Furthermore, it was found that Shroom3 induced Col1A1 expression in cultured corneal cells and that this was attenuated by mutating Shroom3 at the homologous site previously associated with keratoconus [Lappin, 2018; Tariq et al., 2011]. Based on these findings, we hypothesize that Shroom3 expression can regulate the expression of collagen within the cornea and consequently plays an important role in the etiology of keratoconus.

My thesis aims to add to our understanding about how *Shroom3* regulates collagen expression in the cornea. Specifically, it investigates the role of the N-terminal domain found solely in the longest isoform of *Shroom3* and a specific amino acid change within this domain that has been associated with keratoconus.

Chapter 2: Materials and Methods

CRISPR/Cas9 generation of Shroom3 mutants, genotyping, and mouse husbandry

The *Shroom3* mouse mutants used in this study were generated by the Ohio State University (OSU) Genetically Engineered Mouse Modeling Core using the following specific reagents. Two guide RNAs were generated from a commercial source that contain the (Cas9-binding), protospacer adjacent motifs (underlined), and scaffold spacer sequences (5'-TCTCTGAGCAGATTGAAGAAGGG and 5'-CAGTCCGGAGCTCACTGAGTCGG). The donor sequence utilized for targeting codon 59 of the longest isoform of the mouse Shroom3 gene was: 5'-GGACAAAGGAACTGACCCAGGCTGGACACAGAGTCACTGTGGCTCTCTCTCATCTCTCTGAGCAGATTGAAGAAGTGGGCAAAGCTGACTCAGTGAGTTCCGGACTGCAAGCTGGGGACGAAGTCATACACATCAATGAGGTGGCGCTGA. The underlined nucleotide deviates from the endogenous mouse sequence and was designed to provide the change necessary for the glycine to valine (G59V) codon change (Figure 2D). Sequencing results in the region of interest revealed that a total of 4/19 founder animals appeared to have alterations in the regions of interest, three of which included a single mutation that caused the intended coding sequence change (*Shroom3*^{G59V}). Among these three, only progenies from a single founder animal were analyzed in this study. In addition to the intended change, a fourth founder animal was serendipitously found to be missing a single nucleotide positioned 6 base pairs 5' of the intended nucleotide change

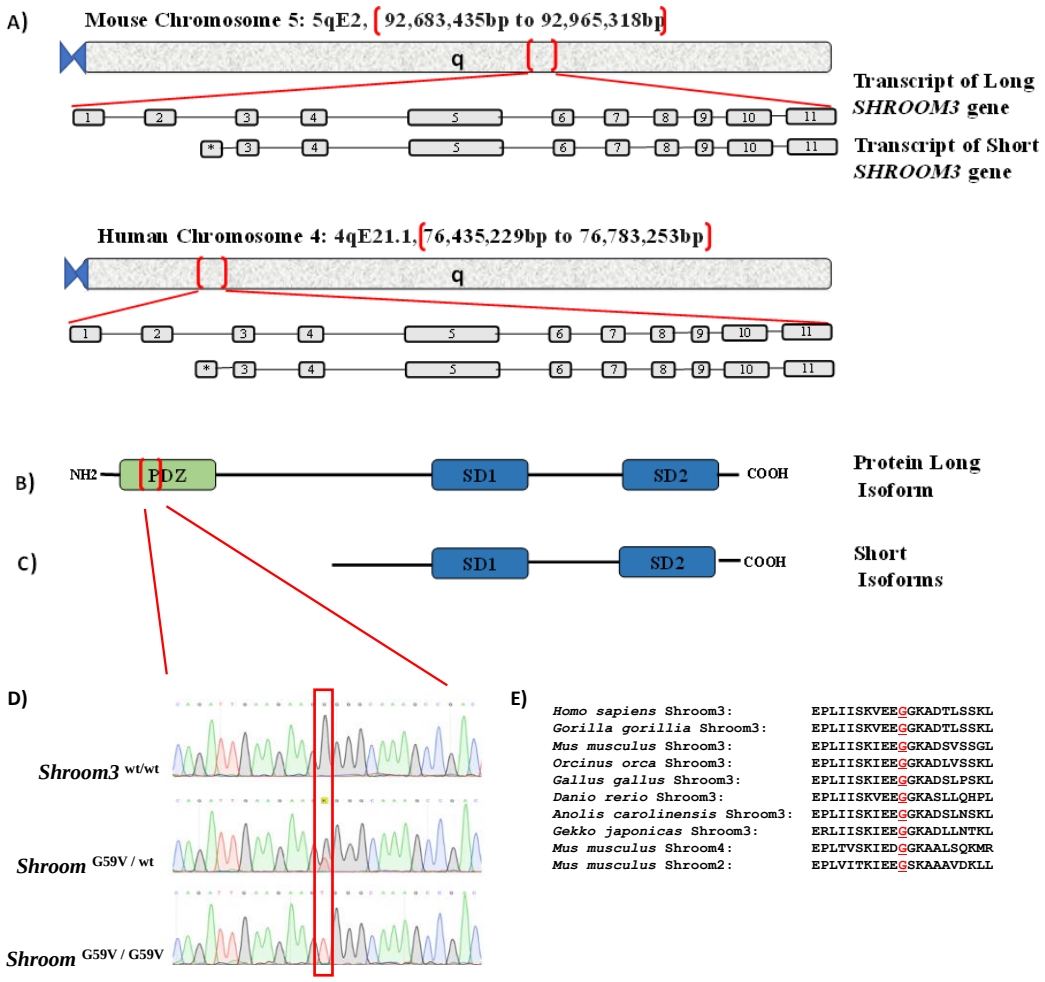

Figure 2. Diagram of the SHROOM3 gene, protein isoforms, chromatogram of G59 line and amino acid sequences of the PDZ region in different species. A) SHROOM3 is located in the long arm of chromosome 5 and 4 in the Homo sapiens and Mus musculus genome, respectively. Its transcription leads to alternatively spliced mRNAs that encode two major Shroom3 isoforms. B) A schematic of the Shroom3 protein structure with its main known domains: PDZ, Shroom Domain 1 (SD1), Shroom Domain 2 (SD2). To date, two isoforms are known with distinct transcriptional start sites. C) Partial chromatogram of G59 line shows mutation of guanine. E) Amino acid sequences of the shroom3 PDZ domain of different species including mouse vs human, the human keratoconus associated mutation was G60V which is analogous to the G59V mutation made in mice.

and is predicted to cause the longest Shroom3 isoform to terminate prematurely and is hereafter referred to as *Shroom$^{\Delta iso1}$*. The genotypes of each animal are determined from genomic PCR of tail snips at weaning using a high fidelity Taq polymerase, the following primers (5'- CCCGGTGCAAGGGGTATGGTT and 5'-TTAGAAGGGACAGGGTTGGCG), and the program (98^{o} for 30 sec (98^{o} for 10 sec., 60^{o} for 30 sec., 72^{o} for 30 sec for 40 cycles), 72^{o} for 10 min). Following PCR, the resulting 320 base pair bands are gel-purified and undergo Sanger sequencing at the Genomics Shared Resource at OSU with one of the primers listed above. The sequence data files are analyzed with the program SnapGene. The animals were housed in a University Laboratory Animal Resource managed vivarium and were handled in compliance with the guidelines of use of the Institutional Animal Care and Use Committee (IACUC) at OSU.

Histology: Corneal Embedding and Slide Preparations

Mice were euthanized by isoflurane or CO_2 inhalation in accordance with IACUC guidelines. Shroom3^{G59V} and Shroom$^{\Delta iso1}$ mice were ten and six months old respectively. Eyes were removed by putting pressure with forceps around the orbit and a small pair of curved forceps are inserted around the globe and pulled so that the optic nerve can be cut, effectively enucleating the eye. Prior to embedding a stereomicroscope was utilized to image the eye perpendicular to the light axis to visualize the corneal thickness and shape of the anterior chamber (see below). The eyes were then placed in a 15% sucrose-PBS (phosphate-buffered saline) solution prepared in 1x PBS at 4^{o}C and

placed on a rotator for at least one hour or until the tissue settled to the bottom of the tube. This process was repeated by placing the eye in a 30% sucrose solution for cryoprotection. Then, the tissue samples were transferred to a petri dish and the excess sucrose solution was removed by using a kimwipe. The eyes were then embedded in Optimal Cutting Temperature compound (Fisher Scientific), frozen using a bath of dry ice and 100% ethanol and stored at -80°C until ready for use. A cryostat microtome (Leica Biosystems Inc.) was used to prepare histological sections of the embedded tissues. The tissue was positioned with the transverse plane parallel to the bottom of the embedding mold, and frozen blocks of tissues were then sectioned along the direction parallel to transverse plane of the eyecup at 10 μm thickness. The slices were adhered to glass slides, which were previously identified with date and a unique mouse identifier number. The number encompassed the sub-strain line the mouse came from and the corresponding number that mouse is in that line. Slides were then stored at -20° C for further use in immunofluorescence stating and/or imaging.

Antibodies, Immunofluorescence Staining, and Imaging

Transversely cryo-sectioned eyes at the level of the cornea placed on glass slides were incubated for one hour at room temperature. This was followed by three consecutive rinsing steps that consisted of submerging slides for 10 minutes in PBS-T (detergent solution of PBS and 0.1% Tween 20, Fisher Scientific) and placing on a rotating platform. The PBS-T was refreshed with each rinse, using new prepared solution. In order to unmask hidden epitopes, an antigen retrieval step was performed by incubating

the slides in a 100 mM, pH 9.0 Tris solution (MP Biomedicals) for 45 minutes, in a commercial kitchen steamer. Three additional 10-minute rinses of PBS-T were carried out, after which the slides were placed on a slide warmer for 10 minutes. Then, two rings of liquid blocker were drawn around each tissue sample using a PAP Pen (Abcam) and returned to the slide warmer until the blocker had dried. The slides were then placed on a damp paper towel and the primary antibody solution was applied until the entire sample was covered. Primary antibodies (Table 1) were prepared in a solution of 4% milk PBS-T and the samples were incubated overnight in 4^{o}C fridge on rocker in humidified chamber. Rabbit anti-Collagen I monoclonal and rabbit anti-Collagen IV monoclonal (ThermoFisher Scientific) antibodies were used for protein detection. Also, we performed immunofluorescent labeling using Shroom3 Iso1 and Iso1/2 isoform antibodies to detect the presence of respective proteins in Shroom$^{\Delta iso1/\Delta iso1}$ and wild type embryonic neuroepithelial tissue. Iso 1/2 antibody detects both isoforms while the Iso1 antibody detects only the longest isoform. β-catenin is an integral structural component of cadherin-based adherens junctions that localizes to the junctions of epithelial cells. The primary antibodies used in the study and their concentrations are listed in Table 1.

Protein	Host	Vendor	Catalog Number	Dilution
Collagen I	rabbit	ThermoFisher	MA1-26771	1:500
Collagen IV	rabbit	ThermoFisher	1282-RBM1-P1ABX	1:500
β-catenin	mouse	Santa Cruz	sc-7199	1:500

Table 1. Primary Antibodies that were used in this study.

The next day, after three 10 minutes PBS-T washes, the slides were incubated with the corresponding secondary antibodies for 2 hours at room temperature. The fluorescently conjugated secondary antibodies, AlexaFluor 488 anti-mouse IgG mouse (Life Technologies, A11001) and AlexaFluor 594 anti-rabbit IgG (Life Technologies, A21207), were used to label the primary antibodies. The secondary antibodies were prepared in a solution of 4% milk PBS-T in a 1:1000 dilution. After incubation, the samples were rinsed thoroughly three times, 10 minutes each, with PBS. The samples were kept in PBS until ready to image. When the samples were ready to use, a coverslip with Fluoro-Gel (Fisher Scientific) was added and stored on a dry humidifier chamber until the coverslips were dried. The samples were kept in dark until ready to image. Images were acquired using a fluorescence microscope, Zeiss LSM 700 Laser Scanning Confocal System w/ Zeiss Observer Z1 Inverted Phase Contrast Fluorescence Microscope (Zeiss, Germany) equipped with a digital camera using imaging software (Zeiss ZEN software). A fluorescent microscope (Olympus IX71; Olympus Corp., Tokyo, Japan) was used to take images of mice corneas.

Measuring topographic parameters of mouse corneas

The enucleated eyes were imaged through stereo microscopy before being transformed into histological sections. The central, mid-peripheral, and peripheral thickness of the cornea, radius of curvature, anterior chamber angle, and anterior chamber cross-sectional area were measured using ImageJ software from images of the enucleated mouse eyes. These parameters were assessed in samples prepared from animals of

Shroom3^{G59V} and *Shroom3*$^{\Delta iso1}$ lines. Both eyes of eight Δiso1 line: four heterozygous (*Shroom3*$^{wt\ \Delta iso1}$) and four homozygous (*Shroom* $^{\Delta iso1/\Delta iso1}$) mice along with seventeen G59V Shroom3 line: three for wild type (*Shroom3*$^{wt/wt}$), four heterozygous (*Shroom3*$^{wt/G59V}$), and ten homozygous (*Shroom3*$^{G59V/G59V}$) animals were evaluated for the study. Thereafter, images were opened using the same program to evaluate quantitative morphometric parameters of a total of 48 images of animal groups as previously described.

Stereomicroscope images of each fixed eye were generated and following adjustments to the scaling parameters (0.247micrometers/pixel), morphometric properties of each the eye were measured. The scale is based on the size of the images taken by the stereomicroscope. Through the manual repetitive tracing of linear segments at exact points along the cornea of the biological image in ImageJ the central, mid-peripheral, and peripheral thickness of the cornea is acquired. In the Analyze tab of ImageJ, a feature known as Kappa, allows the selected picture to be processed into a file allowing for further acquirement of data on corneal features such as the radius of curvature, anterior chamber angle, and anterior chamber cross-sectional area [Hadrien & Brouhard, 2019]. The Kappa function achieves this through drawing a curve from manually sketches equidistance points along the object of interest. The curve is fitted through an algorithm. This allows the user to measure the curvature of the objects. All images were stored in TIFF format, and the central, mid-peripheral, and peripheral thickness of the cornea as well as the other parameters were compared between groups.

To evaluate the corneal thickness quantitatively, five non-overlapping sets of measurements for each sample were taken and the means calculated for all eyes using ImageJ. The cornea was divided into central, periphery, and mid-periphery zones. The central zone was defined from the central point of the cornea at its apex around which the five measurements are repetitively taken. The peripheral zone with a radius of 0.1 to 0.2 mm beginning at the limbus and mid-periphery at the mid distance between the center and periphery. The five measurements are then averaged in each sample for each zone. The resulting mean thickness for each zone was then grouped together in categories: wild type (*Shroom3*$^{wt/wt}$), heterozygous (*Shroom3*$^{wt/G59V}$), and homozygous (*Shroom3*$^{G59V/G59V}$). These groups of data for each category were then compared to determine if a statistically significant difference exists between the three categories.

To quantify corneal curvatures, a line was carefully traced along the anterior outer corneal surface manually. Then, using the Kappa curvature tool of ImageJ, the software's algorithm generated a best fit curve and 5,500-6,500 curvature measurements (um^{-1}). The nearly 6000-point curvatures for each image were exported in CVS files. These point curvatures were then divided into four groups that approximate where along the traced line the points were measured. This data is presented in forms of percentages to encapsulate the collection of points gathered in the peripheral and central cornea. The collection of the points along the traced line that were considered the peripheral curvature encompassed the 0-25% and 75-100% of all points measured. While the central curvature encompassed 26-74% of all points. Radiuses for the peripheral and central cornea were then calculated as the inverse of curvature data (1/cr). The central and peripheral radiuses

were then grouped together in categories: wild type (*Shroom3*$^{wt/wt}$), heterozygous (*Shroom3*$^{wt/G59V}$), and homozygous (*Shroom3*$^{G59V/G59V}$. The categories were then be compared between each other to determine if a difference was present. The corneal area was measured by using anterior chamber depth as a reference. The anterior chamber depth is defined as the distance between the posterior corneal surface to the anterior lens surface [Nilsson et all., 2005]. The anterior chamber depth is used as a guiding source to trace a consistent connected line across the entire posterior surface of the cornea and the entire anterior surface of the lens. The ImageJ outline tool uses the line encapsulating the entirety of the anterior chamber and then spits out the corresponding area value. Using the angle tool in ImageJ, the anterior change angle was measured. The angle was mapped through subjectively identifying the apex of the anterior chamber angle and drawing a line tangential to the posterior surface of the cornea and the anterior surface of the iris [Nilsson et al., 2005].

Quantitative measurements of Collagen I and Collagen IV Expression

Images of immunofluorescent stained corneal cryosections were used to assess type I and IV collagen expression. The samples were collected from six Shroom3$^{\Delta iso1}$ line mice clustered in three groups: Heterozygotes Δiso1/+ (n=2), Homozygotes Δiso1/Δiso1 (n=3), and wild type (n=1) to measure type I collagen expression. Type IV collagen expression was measured on twelve animals splitting in three groups: Heterozygotes Δiso1/+ (n=3), Homozygotes Δiso1/Δiso1 (n=5), and wild type (n=4). Table 6 shows the distribution of samples (slides) used for comparing collagen I and collagen IV

expressions. Images of corneal sections were taken using a Zeiss Observer Inverted Phase Contrast Fluorescence Microscope and Zeiss ZEN software. To evaluate the entire corneal expression of type I and IV collagens, at least three sections for each central zone and both peripheries were prepared and imaged. The sections were determined subjectively after sectioning.

To assess collagen expression ImageJ software was used. The staining intensity of collagen was measured on all corneas. To normalize for collagen intensities, intensity to empty background space was measured in parallel for each sample. This provided a standard intensity for each individual image, and thus allowed for consistency when comparing collagen intensities. Data were reported as the ratio of collagen intensity to empty background space. The intensity ratios were compared between Heterozygotes Δiso1/+, Homozygotes Δiso1/Δiso1, and wild type groups.

Statistical Analyses

Initial analyses included examination of summary statistics tables, confidence intervals, and graphical summaries such as scatterplots. These statistics were carried out for samples on the central, mid-peripheral, and peripheral thickness of the cornea, radius of curvature, anterior chamber angle, and anterior chamber cross-sectional. Descriptive statistics including means, standard deviations, median, quartiles, and confidence intervals were used to describe the data. All statistical analysis were performed using R software, version 4.0.4. A two-tailed t-test was conducted to compare mean differences between two groups. Non-parametric Kruskal Wallis was applied to evaluate correlations

between continuous factors when more than two groups were involved in statistical analysis followed by Tukey's post-hoc test for pairwise comparisons. Ratios of densities to background in type I and IV corneal collagens were expressed as means and ANOVA was used for comparison, followed by Tukey's post-hoc test for pairwise comparisons. Tests were assumed to be statistically significant if the adjusted P values were <.05.

Chapter 3: Results

Assessment of corneal phenotypic characteristics of the Shroom3^{G59V} line

A unique G59V homozygous mutation of *SHROOM3*, identified by whole-exome sequencing in an individual with keratoconus, was previously hypothesized to cause the corneal pathology [Tariq et al., 2011]. To test whether this genomic change has any effect on the cornea, a homologous mutation was generated in mice. While previous studies have commonly demonstrated that the stroma becomes thinner in keratoconus patients, especially in severe cases [Reinstein et al., 2010; Gromacki & Barr, 1994], alterations of other parameters within the anterior chamber, such as the anterior angle and depth are noted [Emre et al., 2007]. Therefore, as a first step in this analysis, the morphometric corneal features of the *Shroom3^{G59V}* mouse line were assessed.

The central, mid-peripheral, and peripheral thickness of the cornea, radius of corneal curvature, anterior chamber angle, and anterior chamber cross-sectional area were measured for wild-type (*Shroom3$^{wt/wt}$*), heterozygous (*Shroom3$^{wt/G59V}$*), and homozygous (*Shroom3$^{G59V/G59V}$*) animals (Figure 3A). For this experiment the eyes of 10-month-old, inbred mice from the *129S1/SvImJ* substrain were used. In all genotypes examined, the average total corneal thickness was thicker centrally and became increasingly thinner towards the peripheral cornea (Table 2). Central, mid-periphery, and peripheral corneal mean thickness were found to be 102.9 ± 6.9μm, 97.7 ± 3.4μm, 87.3 ± 3.7μm in wild type mice.

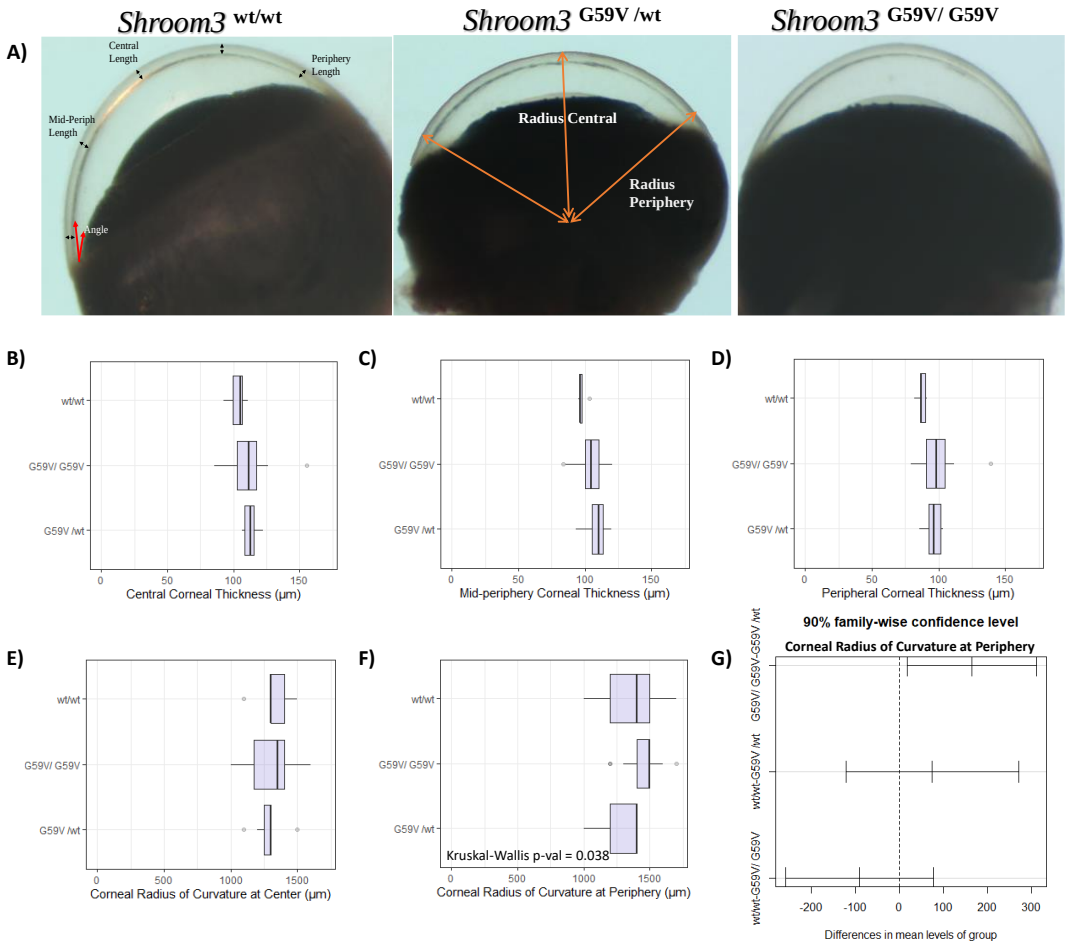

continued

Figure 3. Comparison of corneal morphometric parameters in Shroom3 mice. A) Representative images of dissected eyes from wild type (Shroom3$^{+/+}$), heterozygous (Shroom3$^{+/G59V}$), and homozygous (Shroom3$^{G59V/G59V}$) mice. Quantitative comparison of central corneal thickness (B), mid-peripheral thickness (C), peripheral thickness (D), radius of curvature at center (E) showed no significant differences among three groups using Kruskal-Wallis's test. A significant difference was detected using Kruskal-Wallis's when comparing among groups for (F) peripheral radius measurements. (G) Tukey was used to further compare the difference among pair groups. It shows that difference remains between mutant and heterozygous groups. No significant differences for anterior chamber angle (H) and area (I) were observed.

Figure 3 continued

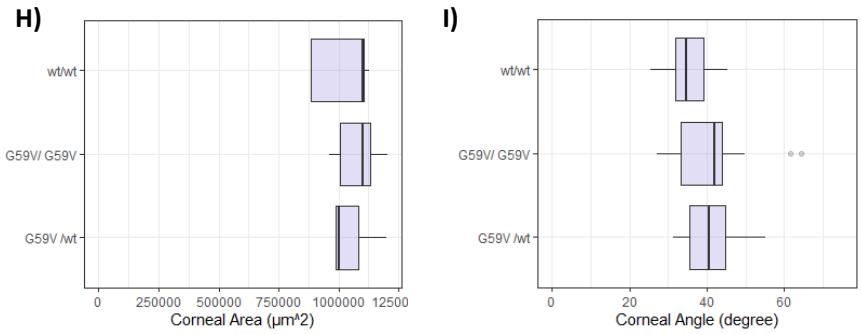

In *Shroom3*$^{wt/G59V}$ mice the central, mid-periphery, and peripheral corneal mean thickness measurements were 112.8 ± 5.4µm, 108.7 ± 8.8µm, 96.1 ± 6.7µm, respectively in *Shroom3*$^{wt/G59V}$ mice, while in *Shroom3*$^{G59V/G59V}$ mice they were found to be 111.4 ± 14.7µm, 101.6 ± 9.9µm, 98.2 ± 13.2µm, respectively. Corneal radius of curvature at the center and periphery measured 1,320.0 ± 148.2µm and 1,360.0 ± 270.2µm, respectively, in wild type mice. In in *Shroom3*$^{wt/G59V}$ mice they were 1,285.7 ± 121.4µm and 1,285.7 ± 158.8µm, respectively, while in *Shroom3*$^{G59V/G59V}$ mice they were found to be 1,310.0 ± 165.1µm and 1,450.0 ± 119.2µm, respectively. The angle of the anterior chamber measured 35.2 ± 7.5, 41.1 ± 8.1, and 41.0 ± 9.8 degrees for wild-type mice (*Shroom3*$^{wt/wt}$), *Shroom3*$^{wt/G59V,}$ *and Shroom3*$^{G59V/G59V}$, respectively. Anterior chamber cross-sectional areas were found to be 1,020,560 ± 124,539 µm^2, 1,048,154 ± 81,124 µm^2, and 1,078,315 ± 71,021 µm^2 for wild-type mice, *Shroom3*$^{wt/G59V}$ and *Shroom3*$^{G59V/G59V}$, respectively.

A statistical analysis revealed no significant difference in central (p = 0.129), mid-peripheral (p = 0.085), and peripheral (p = 0.092) corneal thickness between the wild type, heterozygous, and homozygous *Shroom3*^{G59V} mutants (Figure 3B, 3C, 3D). When

comparing the three groups in radius of curvature (p = 0.777), in corneal angle of the anterior chamber (p = 0.504), and in area (p = 0.459), no significant differences were observed (Figure 3E, 3H, 3I). A significant difference was found among all groups for (Figure 3F) peripheral radius of curvature using Kruskal-Wallis for multigroup comparison (p = 0.038). Furthermore, Tukey's HSD Test for pairwise comparisons (Figure 3G) indicated that the mean value of radius curvature at periphery was borderline, but not quite significantly different between *Shroom3*$^{wt/G59V}$ and *Shroom3*$^{G59V/G59V}$ eyes (p = 0.059, 90% C.I. = 17.43, 311.12).

	Shroom3 $^{wt/wt}$ **Mean ± SD**	***Shroom3*** $^{wt/G59V}$ **Mean ± SD**	***Shroom3*** $^{G59V/G59V}$ **Mean ± SD**
Observations (eyes)	5	7	20
Central Thickness (µm)	102.9 ± 6.9	112.8 ± 5.4	111.4 ± 14.7
Mid-Peripheral Thickness (µm)	97.7 ± 3.4	108.7 ± 8.8	101.6 ± 9.9
Peripheral Thickness (µm)	87.3 ± 3.7	96.1 ± 6.7	98.2 ± 13.2
Radius of Curvature at Center (µm)	1,320.0 ± 148.2	1,285.7 ± 121.4	1,310.0 ± 165.1
Radius of Curvature at Periphery (µm)	1,360.0 ± 270.2	1,285.7 ± 158.8	1,450.0 ± 119.2
Corneal Angle (degree)	35.2 ± 7.5	41.1 ± 8.1	41.0 ± 9.8
Area (µm^2)	1,020,560 ± 124,539	1,048,154 ± 8,1124	1,078,315 ± 71,021

Table 2. Morphometric corneal features of *Shroom3*^{G59V} line.

Overall, no statistically significant difference was found between wild type, *Shroom3*$^{G59V/G59V}$ (p=.491, 90% C.I. = -275.21, 77.21), and *Shroom3*$^{wt/G59V}$ groups (p=.699, 90% C.I. = -121.52, 311.12) for radius of curvature at periphery. The p-values

for all comparisons are shown in Table 3. Altogether these results show that the amino acid change (G59V) does not substantially alter corneal measurements in the eyes of homozygous or heterozygous mice.

	Wild Type (N)	*Shroom3* $^{G59V/+}$ (N)	*Shroom3* $^{G59V/G59V}$ (N)	*P***	*90% CI*	Total
Radius of Curvature at Periphery	5	7	20	**<0.038***		32
Shroom3 $^{G59V/G59V}$ * *WT*				**0.491**	**-275.21, 77.21**	
Shroom3 $^{G59V/G59V}$ * *Shroom3* $^{G59V/+}$				**0.059**	**17.43, 311.12**	
*WT * Shroom3* $^{G59V/+}$				**0.699**	**-121.52, 311.12**	
Other Topographic Measurements	5	7	20			32
Central Thickness				**0.129**		
Mid-Peripheral Thickness				**0.085**		
Peripheral Thickness				**0.092**		
Radius of Curvature at Center				**0.777**		
Corneal Angle				**0.504**		
Area				**0.459**		

Table 3. P-values of comparison of morphometric corneal measurements in Control vs mutant vs heterozygous *Shroom3*^{G59V} mice.

Analysis of the sequence and expression of Shroom3 with a novel, CRISPR-generated mutation

During the introduction of the G59V mutation into mice using CRISPR gene editing, an unintended sequential change in the coding sequence was generated. This additional mutation, consisting of a deletion to a single nucleotide positioned 6 base pairs from the intron/exon boundary, is thought to cause a frameshift and terminate translation due to an in-frame stop codon (Figure 4). Thus, the long isoform transcript of Shroom3 is predicted to be substantially truncated and missing all the known functional domains of Shroom3. If this occurs, only the shorter isoform of Shroom3 should be expressed.

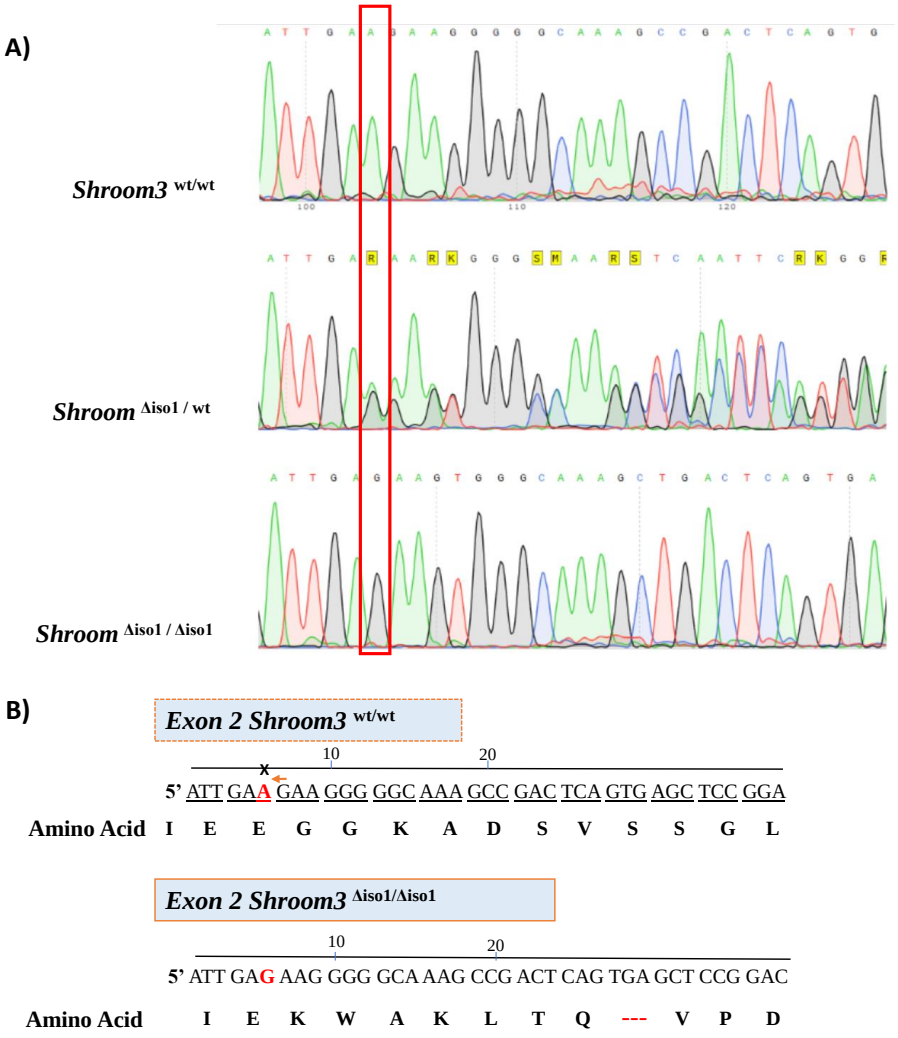

Figure 4. Chromatogram presenting nucleotide sequencing of wild type (Shroom3+/+), heterozygous (Shroom3+/Δiso1), homozygous (Shroom3Δiso1/Δiso1) and amino acid sequences of the PDZ region of wild type and homozygous. A) Sequencing of the Shroom3 PDZ region using chromatography B) A partial sequencing of Shroom wild type Exon 2 (top), which consists of 155 nucleotides. The loss of a nucleotide in position six (A) leads to a frameshift mutation (bottom), subsequently to a truncated protein. Exon 2 encodes for PDZ region of the protein.

To determine the presence and/or absence of the longest isoform of Shroom3 containing the PDZ domain, embryonic neuroepithelial tissue was collected from *Shroom3*$^{\Delta iso1/\Delta iso1}$ and wild type mice. Immunofluorescent labeling was performed using Shroom3 and β-catenin antibodies. The Shroom3 Iso 1/2 antibody detects both isoforms while the Iso1 antibody detects only the longest isoform (Figure 5). β-catenin is an integral structural component of cadherin-based adherens junctions that localizes to the junctions of epithelial cells (Figure 6). Intensities for β-catenin and Shroom3 isoforms were compared qualitatively in embryonic neuroepithelial tissue samples from *Shroom*$^{\Delta iso1/\Delta iso1}$ and wild-type embryos (Figure 6).

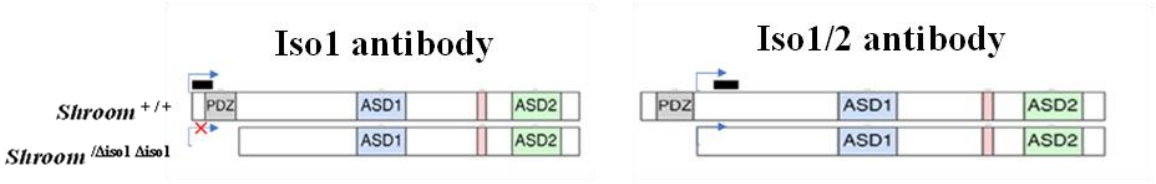

Figure 5. Diagram of the antibody binding sites for each of the Shroom3-specific antibodies. The Iso1 antibody binds to the N-terminus of the Shroom3 protein while the Iso1/2 antibody binds to an antigen found in both isoforms of Shroom3 The antibodies are represented as a black box in the diagram.

Intense immunofluorescent labeling of both the long isoform of Shroom3 and β-catenin (Figure 6A) is detected in the apical neuroepithelial junctions of the wild type samples. However, β-catenin, but not the long isoform of Shroom3, is detected in the junctions of mutant *Shroom*$^{\Delta iso1/\Delta iso1}$ tissue (arrows, Figure 6B). The presence of β-catenin immunofluorescent labeling in both experimental groups indicates that the lack of Shroom3 labeling is not due to the absence of apical junctions.

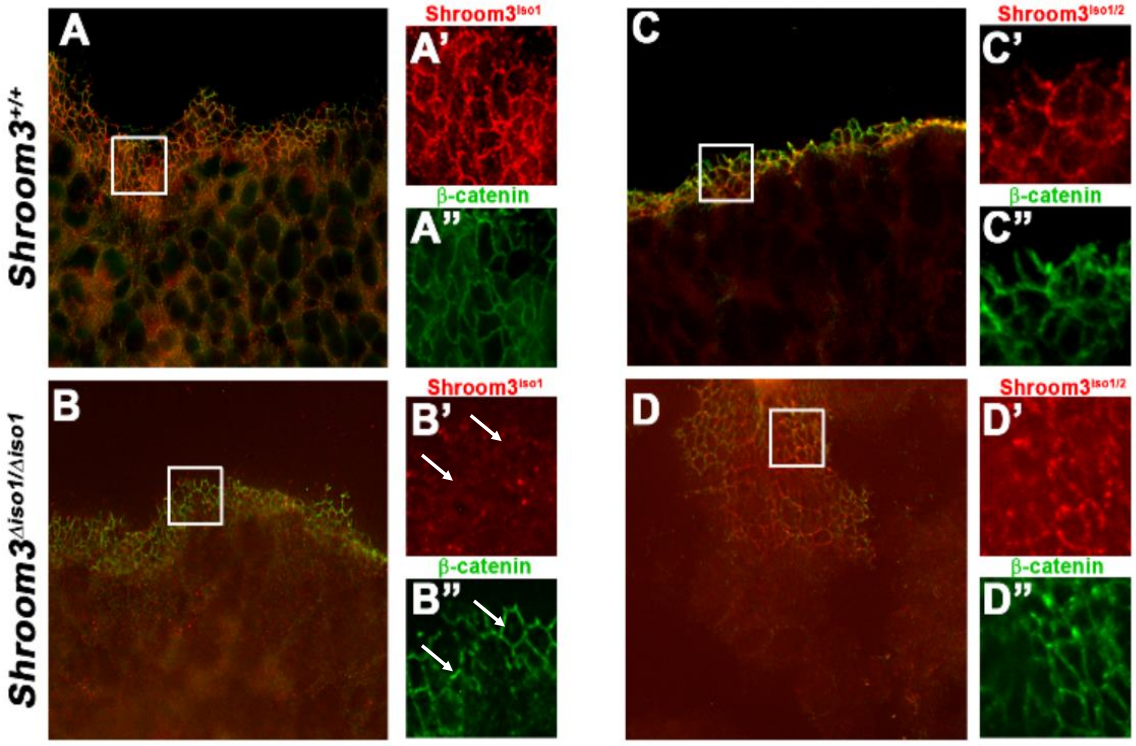

Figure 6. Immunofluorescent staining of embryonic neuroepithelial tissues using distinct Shroom3 antibodies. A-B) An isoform specific Shroom3 antibody (Iso1, red)) that binds to an antigen found only in the longest Shroom3 isoform was used simultaneously with an antibody specific for β-catenin (green) to immunofluorescently label neuroepithelial tissue from wild-type (A) and *Shroom3*$^{\Delta iso1/\Delta iso1}$ (B) mutant embryos. Note that the longest isoform of Shroom3 is detected in the apical junctions of control but not mutant tissue (arrows in B), implying that the longest isoform is not present in the mutant tissue. C-D) In contrast, a distinct Shroom3 antibody (Iso1/2, red) that binds to an antigen found in both the long and short Shroom3 isoforms was used simultaneously with an antibody specific for β-catenin (green) to immunofluorescently label neuroepithelial tissue from wild-type (C) and *Shroom3*$^{\Delta iso1/\Delta iso1}$ mutant (D) embryos. Note that Shroom3 and β-catenin is detected in the apical junctions of tissue from both genotypes.

The isoform specific Shroom3 antibody (Iso1, red)) that binds to an antigen found only in the longest Shroom3 isoform was used to immunofluorescently label neuroepithelial tissue from wild-type and *Shroom3*$^{\Delta iso1/\Delta iso1}$ mutant embryos. The longest isoform of Shroom3 is detected in the apical junctions of control but not mutant tissue (Figure 6B), implying that the longest isoform is not present in the mutant tissue Furthermore, the presence of Shroom3 labeling in tissues from both genotypes using the Shroom3$^{Iso1/2}$ antibody suggests that expression of the shorter isoform is unaffected which further implies that the longest isoform is not present in the mutant tissue.

Assessment of corneal phenotypic characteristics of the Shroom3 $^{\Delta iso1}$ *line*

With the potential absence of the longest isoform in *Shroom3*$^{\Delta iso1/\Delta iso1}$ mice**,** the door is open to investigate a specific role for the longest isoform in the development of keratoconus and/or corneal structure. The central, mid-peripheral, and peripheral thickness of the cornea, radius of curvature, anterior chamber angle, and anterior chamber cross-sectional area were measured for heterozygous (*Shroom3*$^{wt/\Delta iso1}$) and homozygous (*Shroom3*$^{\Delta iso1/\Delta iso1}$) animals using ImageJ imaging software (Figure 7A). For this experiment we used inbred mice from the same substrain, *129S1/SvImJ*, and the eyes came from animals approximately 6 months old.

The mean for the central, mid-periphery, and periphery thickness of the cornea was 115.2 ± 8.1 µm, 107.7 ± 9.7 µm, 95.1 ± 15.0 µm, respectively in *Shroom3*$^{wt/\Delta iso1}$ mice. In *Shroom3*$^{\Delta iso1/\Delta iso1}$ mutant these measures were in turn 105.7 ± 7.3 µm, 105.2 ±

12.2 µm, 92.4 ± 8.8 µm. A significant difference ($p < 0.05$, 90% C.I. = -4.19, -0.62) was observed when comparing the central thickness between *Shroom3*$^{wt/\Delta iso1}$ and *Shroom3*$^{\Delta iso1/\Delta iso1}$ mutants (Figure 7B).

As expected, the cornea was thicker centrally and became increasingly thinner towards the peripheral cornea in both heterozygous and homozygous Δiso1 mutants. Of note, in the *Shroom3*$^{wt/\Delta iso1}$ group total corneal thickness at the corneal vertex was, on average, 20.1 µm thicker than at the periphery, which corresponds to an 18% decrease in thickness between the central and peripheral cornea. In contrast, in *Shroom3*$^{\Delta iso1/\Delta iso1}$ mutant the difference of the total corneal thickness at the corneal vertex compared with the periphery was 12%, being, on average, 13.31 µm thicker (Table 4).

	Shroom3 $^{wt/\Delta iso1}$ **Mean ± SD**	***Shroom3*** $^{\Delta iso1/\Delta iso1}$ **Mean ± SD**
Observations (eyes)	8	8
Central Thickness (µm)	115.2 ± 8.1	105.7 ± 7.3
Mid-Peripheral Thickness (µm)	107.7 ± 9.7	105.2 ± 12.2
Peripheral Thickness (µm)	95.1 ± 15.0	92.4 ± 8.8
Radius of Curvature at Center (µm)	1,220.6 ± 240.4	1,113.7 ± 240.1
Radius of Curvature at Periphery (µm)	1,036.9 ± 201.4	1,127.054 ± 252.2
Corneal Angle (degree)	42.9 ± 6.5	36.1 ± 5.7
Area (µm^2)	1,079,792 ± 95,695	1,057,545 ± 111,687

Table 4. Morphometric corneal features of *Shroom3*$^{\Delta iso1}$ line.

These results indicate a decrease of the average corneal thickness in the samples collected from eyes of *Shroom3*$^{\Delta iso1/\Delta iso1}$ mutant, suggesting there is more thinning in the central zone of the mutant lacking the longest isoform of Shroom3 containing the PDZ domain.

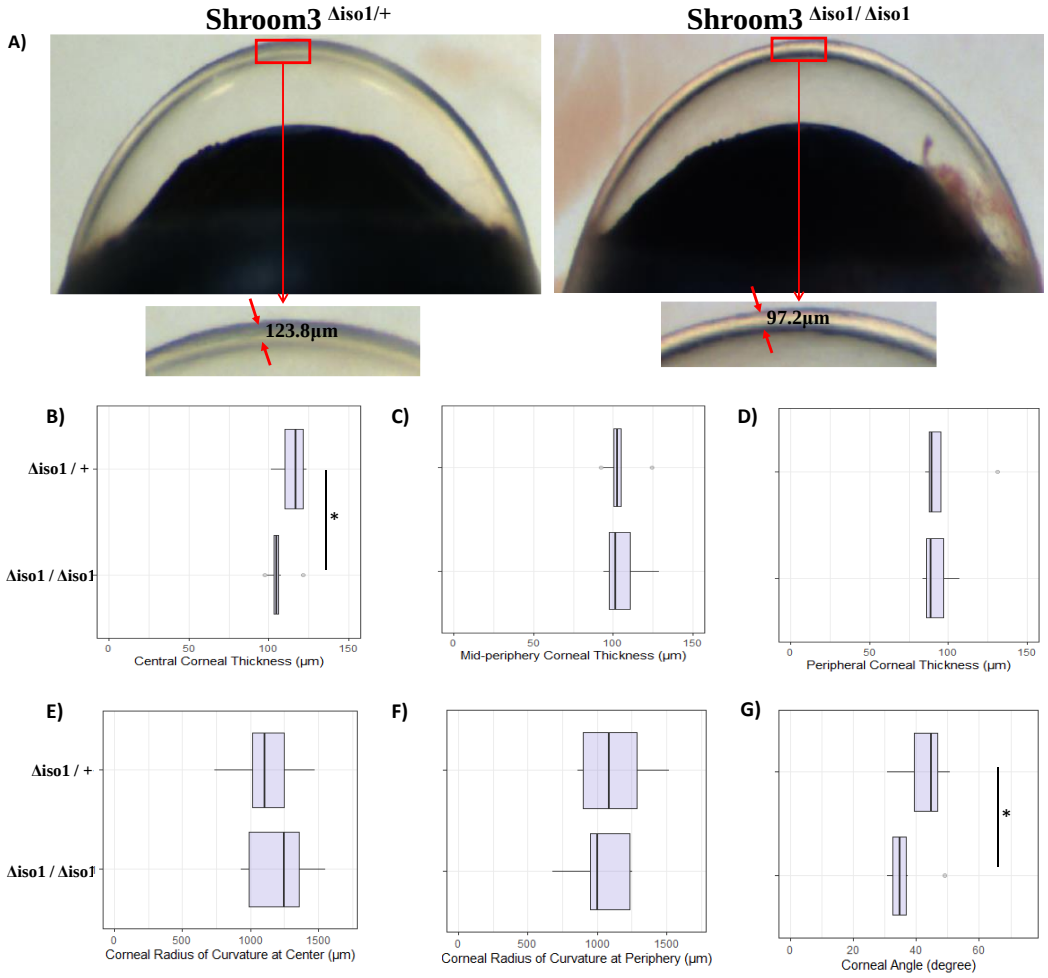

Figure 7. Thickness, Radii and Angles compared in Δiso1 line between groups that undergo frameshift mutation: Heterozygotes$^{Δiso1/+}$ and Homozygotes$^{Δiso1/Δiso1}$. A) Representative images of dissected eyes from heterozygous (Shroom3$^{+/Δiso1}$) and homozygous (Shroom3$^{Δiso1/Δiso1}$) mice. Quantitative comparison of morphometric data for central corneal thickness (B) and angle (G) shows significant differences among two groups, p-values < 0.05, while there are no differences for mid-periphery (C) and peripheral (D) corneal thickness as well as for Radii: central (E) and periphery (F).

The radius of curvature at the center and periphery of the cornea were measured 1,220.6 ± 240.4μm and 1,036.9 ± 201.4μm, respectively, in *Shroom3*$^{wt/\Delta iso1}$ mutant, while in *Shroom3*$^{\Delta iso1/\Delta iso1}$ samples they were 1,113.7 ± 240.1μm and 1,127.054 ± 252.2μm, respectively. The angle measurements were 42.9 ± 6.5 and 36.1 ± 5.7 degrees for *Shroom3*$^{wt/\Delta iso1}$ and *Shroom3*$^{\Delta iso1/\Delta iso1}$ mutants, respectively. There was a statistically significant difference ($p < 0.05$, 90% C.I. = -13.43, -0.45) between the angle of the heterozygous mutant compared to the homozygous mutant (Figure 7G). Statistical analysis showed no significant difference in mid-periphery ($p = 0.721$, 90% C.I. = -7.97, 12.16) and peripheral ($p = 0.714$, 90% C.I. = -6.89, 7.25) corneal thickness between heterozygous and homozygous Δiso1 mutants (Figure 7C, 7D). Also, no significant differences are found when comparing the two groups for (Figure 7E) corneal radius at center ($p = 0.431$, 90% C.I. = -129.43, 374.45) and (Figure 7F) corneal radius at periphery ($p = 0.874$, 90% C.I. = -293.43, 112.45). Table 5 presents p-values for comparisons between homozygous and heterozygous Δiso1 line groups that undergo the frameshift mutation.

	Wild Type **(N)**	***Shroom3*** $^{\Delta iso1/+}$ **(N)**	***Shroom3*** $^{\Delta iso1/\Delta iso1}$ **(N)**	***P*****	***90% CI***	**Total**
Topographic Corneal Measurements		8	8			16
Central Thickness				**0.031***	**-4.19, -0.62**	
Mid-Peripheral Thickness				**0.721**	**-7.97, 12.16**	
Peripheral Thickness				**0.714**	**-6.89, 7.25**	
Radius of Curvature at Center				**0.431**	**-129.43, 374.45**	
Radius of Curvature at Periphery				**0.874**	**-293.43, 112.45**	
Corneal Angle				**0.041***	**-13.43, -0.45**	

Table 5. P-values of comparison of morphometric corneal measurements in *Shroom3*$^{\Delta iso1}$ line between groups that undergo frameshift mutation.

Quantitative measurement of type I collagen in developing corneas

Type I collagen is abundant in the cornea and is an important component of the stroma. Significantly reduced *COL1A1* mRNA transcript levels are observed when Shroom3 expression is reduced in human kidney cells [Menon et al., 2015]. Furthermore, type I collagen protein expression was reduced in the posterior stroma of *Shroom3* deficient embryos [Lappin, 2018]. For these reasons it is hypothesized that the presence of Shroom3 can regulate collagen expression. To determine whether collagen expression was affected in the homozygous *Shroom3*$^{\Delta iso1/\Delta iso1}$ mutants immunofluorescent labeling was performed using an antibody against collagen type I. Qualitatively, a reduction of collagen I was noted in Shroom*3*$^{\Delta iso1/\Delta iso1}$ cornea. Subsequent fluorescent imaging (Figure 8A) of corneal sections from *Shroom3*$^{\Delta iso1/\Delta iso1}$ (33 images from three different 6-month-old mouse), *Shroom3*$^{\Delta iso1/+}$ (15 images from 2 different 6-month-old mouse), and wild-type (12 images, one 6-month-old mouse) mice (Table 6) was performed. Fiji software was used to quantify the intensity of the Collagen I signal. The quantitative values were normalized. Collagen I intensities were compared between Shroom*3*$^{+/+}$, *Shroom3*$^{\Delta iso1/+}$ and *Shroom3*$^{\Delta iso1/\Delta iso1}$ corneas.

A statistically significant and relatively strong correlation ($p < 0.05$) was found between the intensity of type I collagen and Δiso1 mice (Figure 8B), using ANOVA. To further investigate the correlation within each pair of groups, Tukey's HSD test for pairwise comparisons (Figure 8C) was used. The mean value of type I collagen intensity was significantly different between *Shroom3*$^{\Delta iso1/\Delta iso1}$ when compared with wild

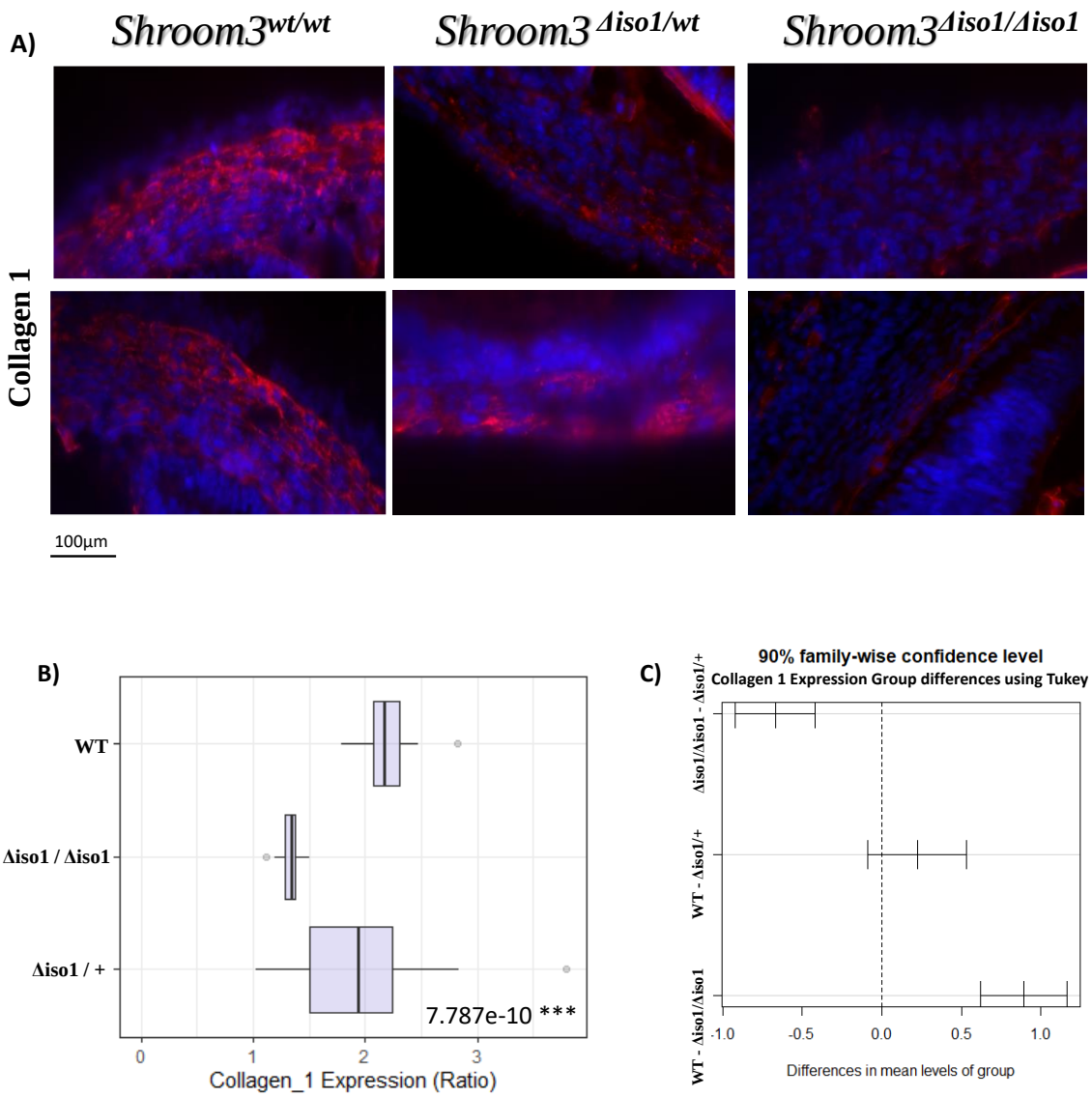

Figure 8. Type I collagen 1 expression in wild type and Shroom3 mutated mouse. Hoechst dye, blue stain specific for nuclei of cells, and red stain shows collagen presence. A) Immunofluorescent staining against type I collagen showed less intensity in corneal tissue of Shroom3$^{\Delta iso1/\Delta iso1}$ mice. B) Quantitative measurement shows statistical significance for less expressed Collagen I among groups using ANOVA ($p < 0.001$). C) Tukey shows a significant difference of the means for the Shroom3$^{\Delta iso1/\Delta iso1}$ when compared with wild type and Shroom3$^{\Delta iso1/+}$ groups. There is no significant difference between the wild type and Shroom3$^{\Delta iso1/+}$.

type ($p < 0.05$, 90% C.I. = -0.92, -0.42) and *Shroom3* $^{\Delta iso1/+}$ ($p < 0.05$, 90% C.I. = 0.62, 1.16). The strong reduction in staining intensity observed in the *Shroom3*$^{\Delta iso1/\Delta iso1}$ mutant in comparison to both heterozygous and wildtype indicates that Shroom3 plays a role in the regulation of regulation of corneal type I collagen. The data suggests that the frameshift mutation, which lead to loss of the PDZ domain, may alter translation of the Shroom3 longest isoform. The data supports that the longest isoform plays a positive role in the expression of type 1 collagen.

The study found no significant difference in type I collagen expression between the wild type and heterozygous groups ($p = 0.3$, 95% C.I. = -0.09, 0.53). The lack of difference in staining intensity between *Shroom3*$^{\Delta iso1/+}$ and wild type indicates that collagen is still being produced in the heterozygous mutant. It implies that the longest isoform of Shroom3 is still being translated in *Shroom3*$^{\Delta iso1/+}$ and is not affecting the regulation of corneal collagen I. Taken together, these results suggest that Shroom3 regulates type I collagen expression in the mouse cornea. For this expression to happen, the Shroom3 longest isoform is required, which hints to a crucial role the PDZ domain may have in translation.

	Wild Type (N)	*Shroom3* $^{\Delta iso1/+}$ (N)	*Shroom* $^{\Delta iso1/\Delta iso1}$ (N)	*P***	*90% CI*	Total
Collagen I	12	15	33	**<0.001*** **		54
Shroom3 $^{\Delta iso1/\Delta iso1}$ **** WT***				**<0.001*** **	**-0.92, -0.42**	
Shroom3 $^{\Delta iso1/\Delta iso1}$ **** Shroom3*** $^{\Delta iso1/+}$				**<0.001*** **	**0.62, 1.16**	
WT * Shroom3 $^{\Delta iso1/+}$				**0.3**	**-0.09, 0.53**	
Collagen IV	38	50	30	**<0.001*** **		118
Shroom3 $^{\Delta iso1/\Delta iso1}$ **** WT***				**<0.001*** **	**0.25, 0.40**	
Shroom3 $^{\Delta iso1/\Delta iso1}$ **** Shroom3*** $^{\Delta iso1/+}$				**<0.001*** **	**-0.43, -0.25**	
WT * Shroom3 $^{\Delta iso1/+}$				**0.92**	**-0.10, 0.07**	

Table 6. P-values of comparison of type I and IV collagen expression in Δiso1 line between groups that undergo frameshift mutation.

Quantitative measurement of type IV collagen in Shroom$^{\Delta iso1}$ line

Although type I collagen is a major component of the corneal stroma of different species [Nakayasu et al., 1986; Myllyharju & Kivirikko, 2004; Henriksson et al., 2009], other collagen types are also present. Type IV collagen is expressed in the basement membrane of the corneal epithelium and in Descemet's membrane but is not normally found in the stroma [Nakayasu et al., 1986]. One manuscript reported that collagen IV expression increased by fibroblastic cells in the stroma of injured rabbit corneas [Ishizaki et al., 1997]. It suggests that stromal fibroblasts may contribute to the formation of basal lamina-like structures in injured corneas [Ishizaki et al., 1997]. A recent study [Lappin, 2018] demonstrated that type IV collagen expression was increased in SIRC cells, similar to fibroblast, exogenously expressing mutant variants of Shroom3. Because we detected an alteration in collagen type I expression the idea that Shroom3 affects the expression of another collagen type was assessed.

To determine whether a change in type IV collagen expression was seen, the corneas of *Shroom3* Δiso line are utilized. Immunofluorescent labeling for collagen IV

was performed on Shroom3$^{\Delta iso1/\Delta iso1}$ (30 images, five 6-month-old), *Shroom3*$^{\Delta iso1/+}$ (50 images, three 6-month-old), and wild type (38 images, four 6-month-old) mice (Table5). Collagen IV intensities were compared between groups of *Shroom3*$^{\Delta iso1/\Delta iso1}$, *Shroom3*$^{\Delta iso1/+}$ and wild type corneas.

A statistically significant and relatively strong correlation ($p < 0.05$) was found between the intensity of type IV collagen staining and Δiso1mutant mice (Figure 9B), using ANOVA. To further investigate the correlation within each pair of groups, Tukey's HSD Test for pairwise comparisons (Figure 9C) was used. The mean value of collagen IV staining intensity was significantly different between *Shroom*$^{\Delta iso1/\Delta iso1}$ when compared with wild type ($p < 0.05$, 90% C.I. = 0.25, 0.40) and *Shroom3*$^{\Delta iso1/+}$ ($p < 0.05$, 90% C.I. = -0.43, -0.25). In contrast to Collagen I, Collagen IV was expressed more in *Shroom3*$^{\Delta iso1/\Delta iso1}$ mutant mice. The increased collagen IV expression observed in the *Shroom*$^{\Delta iso1/\Delta iso1}$ mutant in comparison to both heterozygous and wild type indicates that Shroom3 plays a role in the regulation of type IV collagen.

The data also implies that the downregulation of the Shroom3 longest isoform, due to the frameshift mutation in *Shroom3*$^{\Delta iso1/\Delta iso1}$ mutant, may affect expression of collagen IV. There was no significant difference between the wild type and heterozygous groups ($p = 0.92$, 95% C.I. = -0.10, 0.07). This implies that the Shroom3 longest isoform is still being translated in *Shroom*$^{\Delta iso1/+}$ mutant and therefore, is not affecting the regulation of corneal Collagen IV. Thus, these results suggest that the production of the longest isoform of Shroom3 regulates collagen expression in mice cornea.

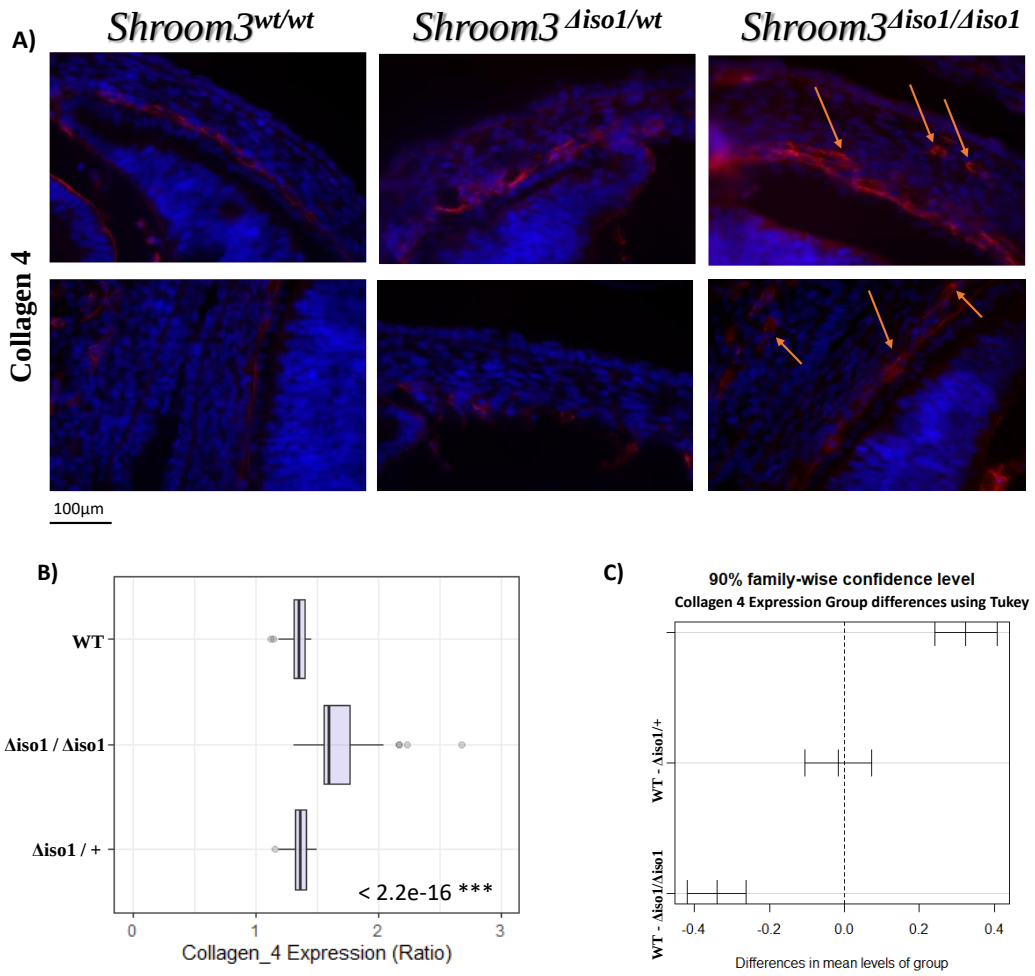

Figure 9. Immunofluorescent labeling of type IV collagen in wild type and Shroom3$^{\Delta iso1/\Delta iso1}$ mutant corneal tissue. A) Immunofluorescent labeling with an antibody specific for type IV collagen (red) and a nuclear dye (Hoechst, blue) reveals the appearance of ectopic, circular type IV collagen positive signal in the central (top) and peripheral (bottom) stroma of mutant but not wild-type corneas. Note that type IV collagen is normally only detected near the endothelium in the wild-type tissue B) Quantitative measurement of type IV collagen fluorescent intensity shows that there is a significant difference in its expression (p-value < 2.2e 16) between groups using ANOVA. C) Tukey statistical testing was used to assess population difference between pairs of groups. It shows a significant difference when comparing the means for the Shroom3$^{\Delta iso1/\Delta iso1}$ with wild type and Shroom3$^{\Delta iso1/+}$ groups. There is no significant difference between the wild type and Shroom3$^{\Delta iso1/+}$.

Chapter 4: Discussion

The G59V mutation of Shroom3 does not alter corneal morphometric measurements

The mouse *Shroom3* gene was altered to substitute the glycine codon for a valine codon at amino acid position 59 in order to mimic a homozygous *SHROOM3* mutation found in a human subject diagnosed with keratoconus [Tariq et al., 2011]. However, the assessment of morphometric corneal features in the Shroom3^{G59V} line of this study failed to uncover any significant differences in corneal thickness (central, mid-peripheral, and peripheral), central corneal curvature, and anterior chamber angle when comparing wild-type (Shroom3$^{wt/wt}$), heterozygous (Shroom3$^{wt/G59V}$), and homozygous (Shroom3$^{G59V/G59V}$) animals. Only a small and insignificant ($p = 0.059$, Table 3) difference was observed between the radii of curvature of the peripheral corneas of the homozygous and heterozygous groups. This difference could be attributed to the small sample size examined in this study. Additionally, the morphometric measurements acquired though Fiji from compiled images could be another factor contributing to this finding. The variation may also be a result of this study's methods which differ from the those utilized in similar studies.

Other documented measurements of corneal parameters, such as corneal thickness, have been acquired using confocal microscopy and low coherence reflectometry. Results using confocal microscopy and reflectometry for central corneal thickness in different mouse strains found 112.9 ± 7.0μm in PEPCK-TGFβ1 wild-type transgenic mice [Jester et al., 2001] and 106 ± 3.45μm in BALB/c mice [Schulz et al.,

2003]. Another study utilizing electron microscopy found central corneal thicknesses of 122.68 ± 4.8, 137.02 ± 14.0, 134.16 ± 12.9μm respectfully amongst three strains of mice (129/SVJ, C57BL/6 and BALB/c) [Henriksson et al., 2009; Henriksson et al., 2012]. It was also determined that peripheral corneal thicknesses among the three strains were 68.00 ± 6.8, 90.55 ± 1.9, 74.48 ± 5.8um peripherally [Henriksson et al., 2009; Henriksson et al., 2012]. The animals in the present study were 10-month-old inbred mice from the same sub strain (129S1/SvImJ) and found that the central corneal thickness ranges from ~103-112μm Therefore, the stereomicroscopy-based methods described here, followed by Fiji imaging analysis on enucleated eyes of mice, appear to be similar to previous studies. However, the data from this study depicts peripheral corneal thickness that ranges from ~87μm to 98.2μm. The difference in peripheral thickness between Henriksson study and this one may also be due to the acquisition of the measurements. The analysis of images gathered through stereo microscopy of enucleated eyes may have been inaccurate because the images were taken in profile and allowed neighboring corneal tissue to possibly distort the image particularly in the peripheral region. This distortion could complicate the precision and accuracy of the tracing process in acquiring data for morphometric parameters. Furthermore, manual line tracing is subjective and thus could be another reason for this discrepancy. However, the central thickness values observed in this study closely matched the measurements from the Henriksson study methods. Thus, it is concluded that the lack of changes in the in the morphometric measurements in the presence of the Shroom3^{G59V} mutation indicate that the G59V mutation alone does not affect corneal development or health.

Although a single homologous and keratoconus-associated missense mutation in Shroom3 does not lead to significant changes in corneal morphometric features in mice, a complex disease like keratoconus might not develop from just one polymorphism. Because Tariq study analyzed only exon sequences, the G60V mutation may have been accompanied with additional changes to intronic sequences within the *SHROOM3* gene itself or other genes. Because Shroom3 expression levels are associated with fibrosis and TGF-beta regulation of collagen in kidney tissue [Menon et al., 2015] it is possible that intronic sequence changes may have also affected Shroom3 expression. It is equally possible that the expression of other keratoconus-associated genes may have been affected. Another contributing factor, and possible avenue for future research, is that *Shroom3* mutant mice may not exhibit pathological changes to the cornea in the same manner as it does in humans. It is possible that given the same genetic or environmental insults, the mouse cornea may not behave in the same manner as human corneas. However, hereditary keratoconus-like phenotypes are observed in the corneas of an inbred mouse strain (SKC) that include a conical appearance and corneal clouding keeping the possibility open [Masayoshi et al., 2002]. Additionally, the age cornea evaluation in mice may also be an explanation for the lack of corneal changes in mice. The onset of clinically diagnosed keratoconus in humans occurs in the second decade [Jiménez, 1997] suggesting that in pathological corneas age might be a contributing factor in the development of keratoconus. While the 10-month-old mice used in this study are relatively old [Fox et al., 2007], this does not necessarily correlate with age in

humans, who live much longer. This is one of the drawbacks that come with the use of mice as model species in keratoconus research.

Shroom3$^{\Delta iso1/\Delta iso1}$ animals lack expression of the long isoform that contains a PDZ domain

The Shroom3 gene produces two major known isoforms using distinct transcriptional start sites from alternative exons. This results in proteins with distinct sizes. The N-terminal PDZ domain, which is conserved in the *Shroom3* gene of multiple species (Figure 3B). is found in Shroom3's long isoform (Figure 2B) but is absent from its short isoform (Figure 2C). The lack of immunofluorescent labeling of mutant tissue with the N-terminus-specific antibody supports the notion that the longest isoform of Shroom3 is not expressed in the *Shroom3$^{\Delta iso1/\Delta iso1}$* homozygous mutants. In contrast, immunofluorescent labeling using an antibody that can detect both long and short isoforms remain unaffected suggesting that the short isoform, which does not contain the N-terminal PDZ domain, is produced normally. The lack of immunofluorescent labeling with the N-terminus specific antibody might be due to a reduced level of the longest isoform that is perhaps below the level of detection. Also, the Shroom3 gene could possibly correct its splicing and still make a long protein that does not contain the antigen and thus would not be recognized by the antibody, but still makes the rest of the protein. This phenomenon can be referred to as exon skipping and can occur in response to single nucleotide polymorphism [Lee et al., 2012]. To confirm the absence of the longest isoform of *Shroom3* an additional test must be performed. The iso1 antibody utilized for

immunofluorescence experiments could be used on western blots of protein lysates collected from the corneas of control and mutant mice to detect the absence or presence of Shroom3's longest isoform in corneal tissue. A lack of long isoform protein expression would confirm whether the Shroom3$^{\Delta iso1}$ mutation is definitively an isoform-specific deletion. Once established this would support the conclusion that the morphological changes observed in the cornea are due to the absence of the longest Shroom3 isoform which contains the PDZ domain.

Shroom3$^{\Delta iso1/\Delta iso1}$ animals have a reduced central corneal thickness and altered anterior chamber angle

The significant reduction observed in the central thickness of Shroom3$^{\Delta iso1/\Delta iso1}$ corneas ($p=0.031$) and the absence of detectable expression of the longest Shroom3 isoform suggests that the longest isoform plays a role in the regulation of corneal thickness. The findings observed in this study support that this change in corneal thickness may be the result of altered collagen expression, a protein essential for corneal structure. It is also possible that disrupted regulation and/or production of collagen may predispose one to develop keratoconus [Kabza et al., 2017]. In support of this notion, collagen and lysyl oxidase expression in corneas from keratoconus patients are significantly decreased [Shetty et al., 2015]. The reduced expression of Collagen type I in the Shroom3$^{\Delta iso1/\Delta iso1}$ mutant corneas we observe are consistent with this possibility. A role for Shroom3 in regulating corneal thickness was also previously suggested to occur by a reduction in

keratocytes within mouse embryonic corneal tissue lacking *Shroom3* [Lappin, 2018]. Because corneal collagens are produced by keratocytes a reduced number of keratocytes might also contribute to thinning of the corneal stroma. Further analyses that compare the number of keratocytes in *Shroom3*$^{\Delta iso1/\Delta iso1}$ wild type corneas will be needed to determine if thickness changes are due to reduced keratocyte number, reduced collagen expression, or both.

The average of the anterior chamber angle was also significantly greater in the homozygous Δiso1 mutant animals when compared to heterozygous mutant ($p<0.05$). This data contrasts with other studies that find the anterior chamber angle to decrease or remain unchanged in cases of severe keratoconus [Emre et al., 2007; Nilsson et al., 2005]. These studies utilized a clinical measurement device (Orbscan) that uses an angle estimation tool to map the angle through identifying the apex of the anterior chamber angle and drawing a line tangential to the posterior surface of the cornea and the anterior surface of the iris [Nilsson et al., 2005]. A similar method was employed in this study, however, the subjective nature in acquiring the data from stereomicroscope images without the aid of a precise clinical tool, may be a source of measurement error. Utilizing more precise clinical tools on the animals may demonstrate changes that are more similar to what is observed in keratoconus.

Collagen expression is dependent on the PDZ domain-containing, long isoform of Shroom3

The present study is the first effort to assess expression of type I and IV collagen in the corneas of animals with isoform specific Shroom3 mutations. The Shroom3 Δiso1 mutation, leads to a reduction in the corneal thickness which may be due in part to an alteration in type I and IV collagen expression. The present study demonstrates ectopic expression of collagen IV and reduced expression of collagen I in the corneas of Shroom3 $^{\Delta iso1/\Delta iso1}$ mutant animals. However, the sample size used in this study for the wildtypes and heterozygotes only are one and two animals respectively. More biological replicates in the wildtypes and heterozygotes Δiso1 groups will need to be performed to confirm the changes observed. Although Type I collagen staining is dramatically reduced in the Shroom3$^{\Delta iso1/\Delta iso1}$ corneas, it remains unclear why the corneas of these animals have a relatively small (but significant) decrease in thickness and remain transparent. One explanation could be the genetic compensation from other collagen genes. The antibody used in this study that detects type I collagen was generated based on the protein sequence translated from the Col1a1 gene. Type I collagen fibrils are made up of a triple helix of 3 proteins: two proteins from Col1a1 and one from Col1a2. [Naomi et al., 2021]. It is possible that the cornea may be able to upregulate Col1a2 when Col1a1 is not expressed at high levels and functionally compensate.

The presence of a PDZ domain specifically within the longest isoform makes it possible that the regulation of collagen expression mediated by Shroom3 may depends on its PDZ domain. How, the PDZ domain may also inhibit production of collagen IV or

increase the production of type I collagen is currently unknown. Many studies have been performed to understand the general function of the PDZ domains. In general, PDZ domains are well-known to mediate protein-protein interactions and play several roles in regulating aspects of cell signaling [Hildebrand et al., 2010; Tariq et al., 2015; Manjunath et al., 2018; Liu & Fuentes, 2019]. In addition, proteins containing PDZ domains may recruit complexes containing several target molecules for the assembly of larger, membrane-bound complexes [Kennedy, 1995; Lee & Zheng, 2010; Tsunada et al., 1997]. Additionally, a more recent study suggests that proteins containing PDZ domain act similarly to mechanotransducer proteins, which are single or complex proteins that assist chemical responses from mechanical stimuli [Bazellières & Le Bivic, 2021]. The mechanotransduction role this protein serves could possibly indicate an unexplored role the PDZ domain may have in regulating collagen expression. It is possible that the PDZ domain may play this role through binding to proteins that stimulate and/or inhibit collagen expression or by facilitating a specific signaling pathway. To determine the protein associated with the domain, a mass spectrometry of an immunoprecipitated corneal lysate with the long isoform specific Shroom3 antibody could be performed.

Chapter 5: Conclusion

This study did not uncover any significant differences in phenotype characteristics, when comparing wild-type (Shroom3$^{wt/wt}$), heterozygous (Shroom3$^{wt/G59V}$) and homozygous (Shroom3$^{G59V/G59V}$), apart from a non-statistical difference in the corneal radius of curvature at the periphery between mutant and heterozygous groups. Therefore, the results of this study do not support the hypothesis that the G59V mutation is sufficient to cause keratoconus. However, the study did show phenotypic alterations such as corneal central thinning and a reduction in the anterior chamber angle in Shroom3$^{\Delta iso1/\Delta iso1}$mice. Additionally, quantitative assessment of collagen expression revealed significant differences within the corneas of Shroom3$^{\Delta iso1/\ \Delta iso1}$ animals. A reduction in type I collagen expression and type IV collagen overexpression in the Δiso1 homozygous mutant in contrast with wild type and heterozygous groups was observed suggesting that the PDZ domain-containing longest isoform of Shroom3 does play an active role in the production of collagen. While some of the methods employed in this study can be improved the results presented here provide a solid starting point to further explore the role of the longest isoform of Shroom3 in collagen expression regulation. It is hypothesized that the N-terminal PDZ regulates and/or expresses collagen through the TGF B-1/SMAD3 pathway.

References

Akhtar, S., Almubrad, T., Paladini, I., & Mencucci, R. (2013). Keratoconus corneal architecture after riboflavin/ultraviolet A cross-linking: ultrastructural studies. *Molecular vision*, *19*, 1526–1537.

Bazellières, E., & Le Bivic, A. (2021). Mechanoregulation of PDZ Proteins, An Emerging Function. *Methods in molecular biology (Clifton, N.J.)*, *2256*, 257–275.

Bergmanson, J. P. G., Doughty, M. J. (2005). Anatomy, morphology and electron microscopy of the cornea and conjunctiva. In: Bennett E, Weissman BA, eds. Clinical Contact Lens Practice. Philadelphia: Lippincott-Williams & Wilkins; 2005;11–39.

Böger, C. A., Gorski, M., Li, M., Hoffmann, M. M., Huang, C., Yang, Q., Teumer, A., Krane, V., O'Seaghdha, C. M., Kutalik, Z., Wichmann, H. E., Haak, T., Boes, E., Coassin, S., Coresh, J., Kollerits, B., Haun, M., Paulweber, B., Köttgen, A., Li, G., … CKDGen Consortium (2011). Association of eGFR-Related Loci Identified by GWAS with Incident CKD and ESRD. *PLoS genetics*, *7*(9), e1002292.

Carlson, E. C., Mamiya, K., Liu, C. Y., Gendron, R. L., Birk, D. E., Funderburgh, J. L., & Kao, W. W. (2003). Role of Cys41 in the N-terminal domain of lumican in ex vivo collagen fibrillogenesis by cultured corneal stromal cells. *The Biochemical journal*, *369*(Pt 3), 461–468.

Chen, S., Mienaltowski, M. J., & Birk, D. E. (2015). Regulation of corneal stroma extracellular matrix assembly. *Experimental eye research*, *133*, 69–80.

Czugala, M., Karolak, J. A., Nowak, D. M., Polakowski, P., Pitarque, J., Molinari, A., Rydzanicz, M., Bejjani, B. A., Yue, B. Y., Szaflik, J. P., & Gajecka, M. (2012). Novel mutation and three other sequence variants segregating with phenotype at keratoconus 13q32 susceptibility locus. *European journal of human genetics: EJHG*, *20*(4), 389–397.

Davidson, A. E., Hayes, S., Hardcastle, A. J., & Tuft, S. J. (2014). The pathogenesis of keratoconus. *Eye (London, England)*, *28*(2), 189–195.

Daxer, A., & Fratzl, P. (1997). Collagen fibril orientation in the human corneal stroma and its implication in keratoconus. *Investigative ophthalmology & visual science*, *38*(1), 121–129.

Deshmukh, H. A., Palmer, C. N., Morris, A. D., & Colhoun, H. M. (2013). Investigation of known estimated glomerular filtration rate loci in patients with type 2 diabetes. *Diabetic medicine: a journal of the British Diabetic Association*, *30*(10), 1230–1235.

Dietz, M.L., Teresa M. Bernaciak, T.M., Vendetti, F., Kielec, J.M., and Hildebrand, J.D. Differential actin-dependent localization modulates the evolutionarily conserved activity of Shroom family proteins. J Biol Chem, 2006. 281(29): p. 20542-54.

Dimasi, D. P., Burdon, K. P., & Craig, J. E. (2010). The genetics of central corneal thickness. *The British journal of ophthalmology*, *94*(8), 971–976.

Dudakova, L., Palos, M., Svobodova, M., Bydzovsky, J., Huna, L., Jirsova, K., Hardcastle, A. J., Tuft, S. J., & Liskova, P. (2014). Macular corneal dystrophy and associated corneal thinning. *Eye (London, England)*, *28*(10), 1201–1205.

Eghrari, A. O., Riazuddin, S. A., & Gottsch, J. D. (2015). Overview of the Cornea: Structure, Function, and Development. *Progress in molecular biology and translational science*, *134*, 7–23.

Emre, S., Doganay, S., & Yologlu, S. (2007). Evaluation of anterior segment parameters in keratoconic eyes measured with the Pentacam system. *Journal of cataract and refractive surgery*, *33*(10), 1708–1712.

Erie, J. C., Patel, S. V., McLaren, J. W., Nau, C. B., Hodge, D. O., & Bourne, W. M. (2002). Keratocyte density in keratoconus. A confocal microscopy study(a). *American journal of ophthalmology*, *134*(5), 689–695.

Eye Bank Association of America. 2019 Eye Banking Statistical Report. 2020. Available at: https://restoresight.org/wp-content/uploads/2020/04/2019- EBAA-Stat-Report-FINAL.pdf. Accessed September 15, 2020.

Farber, M. J., Rizaldy, R., & Hildebrand, J. D. (2011). Shroom2 regulates contractility to control endothelial morphogenesis. *Molecular biology of the cell*, *22*(6), 795–805.

Feizi S. (2018). Corneal endothelial cell dysfunction: etiologies and management. *Therapeutic advances in ophthalmology*, *10*, 2515841418815802. https://doi.org/10.1177/2515841418815802

Fox, J. G., Barthold, S. W., Davisson, M. T., Newcomer, C. E., Quimby, F. W., & Smith, A. L. (2007). *The Mouse in Biomedical Research*. Elsevier Inc.

Fullwood, N. J., Tuft, S. J., Malik, N. S., Meek, K. M., Ridgway, A. E., & Harrison, R. J. (1992). Synchrotron x-ray diffraction studies of keratoconus corneal stroma. *Investigative ophthalmology & visual science*, *33*(5), 1734–1741.

Gomes, J. A., Tan, D., Rapuano, C. J., Belin, M. W., Ambrósio, R., Jr, Guell, J. L., Malecaze, F., Nishida, K., Sangwan, V. S., & Group of Panelists for the Global Delphi Panel of Keratoconus and Ectatic Diseases (2015). Global consensus on keratoconus and ectatic diseases. *Cornea*, *34*(4), 359–369.

Gordon-Shaag, A., Millodot, M., Shneor, E., & Liu, Y. (2015). The genetic and environmental factors for keratoconus. *BioMed research international*, *2015*, 795738.

Greenstein, S. A., & Hersh, P. S. (2021). Corneal Crosslinking for Progressive Keratoconus and Corneal Ectasia: Summary of US Multicenter and Subgroup Clinical Trials. *Translational vision science & technology*, *10*(5), 13.

Gromacki, S. J., & Barr, J. T. (1994). Central and peripheral corneal thickness in keratoconus and normal patient groups. *Optometry and vision science: official publication of the American Academy of Optometry*, *71*(7), 437–441.

Grosse, A. S., Pressprich, M. F., Curley, L. B., Hamilton, K. L., Margolis, B., Hildebrand, J. D., & Gumucio, D. L. (2011). Cell dynamics in fetal intestinal epithelium: implications for intestinal growth and morphogenesis. Development (Cambridge, England), 138(20), 4423–4432.

Gustafsson, I., Bergström, A., Myers, A. C., Ivarsen, A., & Hjortdal, J. (2020). Association between keratoconus disease severity and repeatability in measurements of parameters for the assessment of progressive disease. *PloS one*, *15*(2), e0228992.

Hadrien, M., Brouhard, G. J. Kappa (*κ*): Analysis of Curvature in Biological Image Data using B-splines. (2019). *BioRxiv 852772*; doi: https://doi.org/10.1101/852772

Hagens, O., Ballabio, A., Kalscheuer, V., Kraehenbuhl, J. P., Schiaffino, M. V., Smith, P., Staub, O., Hildebrand, J., & Wallingford, J. B. (2006). A new standard nomenclature for proteins related to Apx and Shroom. BMC cell biology, 7, 18.

Hashemi, H., Heydarian, S., Hooshmand, E., Saatchi, M., Yekta, A., Aghamirsalim, M., Valadkhan, M., Mortazavi, M., Hashemi, A., & Khabazkhoob, M. (2020). The Prevalence and Risk Factors for Keratoconus: A Systematic Review and Meta-Analysis. *Cornea*, *39*(2), 263–270.

Henriksson, J. T., Bron, A. J., & Bergmanson, J. P. (2012). An explanation for the central to peripheral thickness variation in the mouse cornea. *Clinical & experimental ophthalmology*, *40*(2), 174–181.

Henriksson, J. T., McDermott, A. M., & Bergmanson, J. P. (2009). Dimensions and morphology of the cornea in three strains of mice. *Investigative ophthalmology & visual science*, *50*(8), 3648–3654.

Hildebrand, J. D. (2005). Shroom regulates epithelial cell shape via the apical positioning of an actomyosin network. J. Cell Sci. 118, 5191-5203.

Hildebrand, J.D. and P. Soriano (1999). Shroom, a PDZ domain-containing actin-binding protein, is required for neural tube morphogenesis in mice. Cell, 99(5), p. 485-97.

Hughes, A. E., Bradley, D. T., Campbell, M., Lechner, J., Dash, D. P., Simpson, D. A., & Willoughby, C. E. (2011). Mutation altering the miR-184 seed region causes familial keratoconus with cataract. *American journal of human genetics*, *89*(5), 628–633.

Ihalainen A. (1986). Clinical and epidemiological features of keratoconus genetic and external factors in the pathogenesis of the disease. *Acta ophthalmologica. Supplement*, *178*, 1–64.

Ionescu, C., Corbu, C. G., Tanase, C., Jonescu-Cuypers, C., Nicula, C., Dascalescu, D., Cristea, M., & Voinea, L. M. (2016). Inflammatory Biomarkers Profile as Microenvironmental Expression in Keratoconus. *Disease markers*, *2016*, 1243819.

Ishizaki, M., Shimoda, M., Wakamatsu, K., Ogro, T., Yamanaka, N., Kao, C. W., & Kao, W. W. (1997). Stromal fibroblasts are associated with collagen IV in scar tissues of alkali-burned and lacerated corneas. *Current eye research*, *16*(4), 339–348. https://doi.org/10.1076/ceyr.16.4.339.10684

Jemth, P., & Gianni, S. (2007). PDZ domains: folding and binding. *Biochemistry*, *46*(30), 8701–8708.

Kabosova, A., Azar, D. T., Bannikov, G. A., Campbell, K. P., Durbeej, M., Ghohestani, R. F., Jones, J. C., Kenney, M. C., Koch, M., Ninomiya, Y., Patton, B. L., Paulsson, M., Sado, Y., Sage, E. H., Sasaki, T., Sorokin, L. M., Steiner-Champliaud, M. F., Sun, T. T., Sundarraj, N., Timpl, R., … Ljubimov, A. V. (2007). Compositional differences between infant and adult human corneal basement membranes. *Investigative ophthalmology & visual science*, *48*(11), 4989–4999. https://doi.org/10.1167/iovs.07-0654

Kabza, M., Karolak, J. A., Rydzanicz, M., Szcześniak, M. W., Nowak, D. M., Ginter-Matuszewska, B., Polakowski, P., Ploski, R., Szaflik, J. P., & Gajecka, M. (2017). Collagen synthesis disruption and downregulation of core elements of TGF-β, Hippo, and Wnt pathways in keratoconus corneas. *European journal of human genetics: EJHG*, *25*(5), 582–590.

Kaldawy, R. M., Wagner, J., Ching, S., & Seigel, G. M. (2002). Evidence of apoptotic cell death in keratoconus. *Cornea*, *21*(2), 206–209.

Kao, W. W., & Liu, C. Y. (2002). Roles of lumican and keratocan on corneal transparency. *Glycoconjugate journal*, *19*(4-5), 275–285.

Kennedy M. B. (1995). Origin of PDZ (DHR, GLGF) domains. *Trends in biochemical sciences*, *20*(9), 350.

Kennedy, R. H., Bourne, W. M., & Dyer, J. A. (1986). A 48-year clinical and epidemiologic study of keratoconus. *American journal of ophthalmology*, *101*(3), 267–273.

Khaled, M. L., Helwa, I., Drewry, M., Seremwe, M., Estes, A., & Liu, Y. (2017). Molecular and Histopathological Changes Associated with Keratoconus. *BioMed research international*, *2017*, 7803029.

Khawaja, A. P., Rojas Lopez, K. E., Hardcastle, A. J., Hammond, C. J., Liskova, P., Davidson, A. E., Gore, D. M., Hafford Tear, N. J., Pontikos, N., Hayat, S., Wareham, N., Khaw, K. T., Tuft, S. J., Foster, P. J., & Hysi, P. G. (2019). Genetic Variants Associated with Corneal Biomechanical Properties and Potentially Conferring Susceptibility to Keratoconus in a Genome-Wide Association Study. *JAMA ophthalmology*, *137*(9), 1005–1012.

Kim, W. J., Rabinowitz, Y. S., Meisler, D. M., & Wilson, S. E. (1999). Keratocyte apoptosis associated with keratoconus. *Experimental eye research*, *69*(5), 475–481.

Klintworth G. K. (2009). Corneal dystrophies. *Orphanet journal of rare diseases*, *4*, 7.

Komai, Y., & Ushiki, T. (1991). The three-dimensional organization of collagen fibrils in the human cornea and sclera. *Investigative ophthalmology & visual science*, *32*(8), 2244–2258.

Kostyuk, O., Nalovina, O., Mubard, T. M., Regini, J. W., Meek, K. M., Quantock, A. J., Elliott, G. F., & Hodson, S. A. (2002). Transparency of the bovine corneal stroma at physiological hydration and its dependence on concentration of the ambient anion. *The Journal of physiology*, *543*(Pt 2), 633–642.

Köttgen, A., Glazer, N. L., Dehghan, A., Hwang, S. J., Katz, R., Li, M., Yang, Q., Gudnason, V., Launer, L. J., Harris, T. B., Smith, A. V., Arking, D. E., Astor, B. C., Boerwinkle, E., Ehret, G. B., Ruczinski, I., Scharpf, R. B., Chen, Y. D., de Boer, I. H., Haritunians, T., … Fox, C. S. (2009). Multiple loci associated with indices of renal function and chronic kidney disease. *Nature genetics*, *41*(6), 712–717. https://doi.org/10.1038/ng.377

Krachmer, J. H., Feder, R. S., & Belin, M. W. (1984). Keratoconus and related noninflammatory corneal thinning disorders. *Survey of ophthalmology*, *28*(4), 293–322.

Lappin, C. J. (2018). *Investigating the Role of Shroom3 in Collagen Regulation and Development of the Corneal Stroma* [Master's thesis, Ohio State University]. OhioLINK Electronic Theses and Dissertations Center.

Lee, C., Le, M. P., & Wallingford, J. B. (2009). The shroom family proteins play broad roles in the morphogenesis of thickened epithelial sheets. *Developmental dynamic: an official publication of the American Association of Anatomists*, *238*(6), 1480–1491.

Lee, H. J., & Zheng, J. J. (2010). PDZ domains and their binding partners: structure, specificity, and modification. *Cell communication and signaling: CCS*, *8*, 8.

Lee, Y., Gamazon, E. R., Rebman, E., Lee, Y., Lee, S., Dolan, M. E., Cox, N. J., & Lussier, Y. A. (2012). Variants affecting exon skipping contribute to complex traits. *PLoS genetics*, *8*(10), e1002998.

Liu, X., & Fuentes, E. J. (2019). Emerging Themes in PDZ Domain Signaling: Structure, Function, and Inhibition. *International review of cell and molecular biology*, *343*, 129–218.

Lodish, H., Berk, A. and Zipursky, S.L. (2000) Section 24.2 Proto-Oncogenes and Tumor-Suppressor Genes. Molecular Cell Biology. 4th Edition, W. H. Freeman, New York.

Lwigale, P. Y., Cressy, P. A., & Bronner-Fraser, M. (2005). Corneal keratocytes retain neural crest progenitor cell properties. *Developmental biology*, *288*(1), 284–293.

Määttä, M., Heljasvaara, R., Sormunen, R., Pihlajaniemi, T., Autio-Harmainen, H., & Tervo, T. (2006b). Differential expression of collagen types XVIII/endostatin and XV in normal, keratoconus, and scarred human corneas. *Cornea*, *25*(3), 341–349.

Määttä, M., Väisänen, T., Väisänen, M. R., Pihlajaniemi, T., & Tervo, T. (2006a). Altered expression of type XIII collagen in keratoconus and scarred human cornea: Increased expression in scarred cornea is associated with myofibroblast transformation. *Cornea*, *25*(4), 448–453.

Manjunath, G. P., Ramanujam, P. L., & Galande, S. (2018). Structure function relations in PDZ-domain-containing proteins: Implications for protein networks in cellular signalling. *Journal of biosciences*, *43*(1), 155–171.

Mantelli, F., Mauris, J., & Argüeso, P. (2013). The ocular surface epithelial barrier and other mechanisms of mucosal protection: from allergy to infectious diseases. *Current opinion in allergy and clinical immunology*, *13*(5), 563–568. https://doi.org/10.1097/ACI.0b013e3283645899

Martínez-Abad, A., & Piñero, D. P. (2017). New perspectives on the detection and progression of keratoconus. *Journal of cataract and refractive surgery*, *43*(9), 1213–1227.

Masayoshi Tachibana, Wakako Adachi, Shigeru Kinoshita, Yasuhito Kobayashi, Yoshio Honma, Hiroshi Hiai, Yoshibumi Matsushima; Androgen-Dependent Hereditary Mouse Keratoconus: Linkage to an MHC Region. *Invest. Ophthalmol. Vis. Sci.* 2002;43(1):51-57.

Mathew, J. H., Goosey, J. D., Söderberg, P. G., & Bergmanson, J. P. (2015). Lamellar changes in the keratoconic cornea. *Acta ophthalmologica*, *93*(8), 767–773.

Mayo Foundation for Medical education and research. Retrieved from: https://www.mayoclinic.org/diseases-conditions/keratoconus/symptoms-causes/syc-20351352

McMonnies C. W. (2005). The biomechanics of keratoconus and rigid contact lenses. *Eye & contact lens*, *31*(2), 80–92.

Meek, K. M., & Boote, C. (2009). The use of X-ray scattering techniques to quantify the orientation and distribution of collagen in the corneal stroma. *Progress in retinal and eye research*, *28*(5), 369–392.

Meek, K. M., & Knupp, C. (2015). Corneal structure and transparency. *Progress in retinal and eye research*, *49*, 1–16.

Meek, K. M., Blamires, T., Elliott, G. F., Gyi, T. J., & Nave, C. (1987). The organisation of collagen fibrils in the human corneal stroma: a synchrotron X-ray diffraction study. *Current eye research*, *6*(7), 841–846.

Meek, K. M., Tuft, S. J., Huang, Y., Gill, P. S., Hayes, S., Newton, R. H., & Bron, A. J. (2005). Changes in collagen orientation and distribution in keratoconus corneas. *Investigative ophthalmology & visual science*, *46*(6), 1948–1956.

Menon, M. C., Chuang, P. Y., Li, Z., Wei, C., Zhang, W., Luan, Y., Yi, Z., Xiong, H., Woytovich, C., Greene, I., Overbey, J., Rosales, I., Bagiella, E., Chen, R., Ma, M., Li, L., Ding, W., Djamali, A., Saminego, M., O'Connell, P. J., … Murphy, B. (2015). Intronic locus determines SHROOM3 expression and potentiates renal allograft fibrosis. *The Journal of clinical investigation*, *125*(1), 208–221.

Mocan, M. C., Yilmaz, P. T., Irkec, M., & Orhan, M. (2008). In vivo confocal microscopy for the evaluation of corneal microstructure in keratoconus. *Current eye research*, *33*(11), 933–939.

Mohammadpour, M., Heidari, Z., & Hashemi, H. (2017). Updates on Managements for Keratoconus. *Journal of current ophthalmology*, *30*(2), 110–124.

Morishige, N., Petroll, W. M., Nishida, T., Kenney, M. C., & Jester, J. V. (2006). Noninvasive corneal stromal collagen imaging using two-photon-generated second-harmonic signals. *Journal of cataract and refractive surgery*, *32*(11), 1784–1791.

Morishige, N., Wahlert, A. J., Kenney, M. C., Brown, D. J., Kawamoto, K., Chikama, T., Nishida, T., & Jester, J. V. (2007). Second-harmonic imaging microscopy of normal human and keratoconus cornea. *Investigative ophthalmology & visual science*, *48*(3), 1087–1094.

Myllyharju, J., & Kivirikko, K. I. (2004). Collagens, modifying enzymes and their mutations in humans, flies and worms. *Trends in genetics: TIG*, *20*(1), 33–43.

Nakayasu, K., Tanaka, M., Konomi, H., & Hayashi, T. (1986). Distribution of types I, II, III, IV and V collagen in normal and keratoconus corneas. *Ophthalmic research*, *18*(1), 1–10.

Nakayasu, K., Tanaka, M., Konomi, H., & Hayashi, T. (1986). Distribution of types I, II, III, IV and V collagen in normal and keratoconus corneas. *Ophthalmic research*, *18*(1), 1–10.

Naomi R, Ridzuan PM, Bahari H. Current Insights into Collagen Type I. *Polymers (Basel)*. 2021;13(16):2642. Published 2021 Aug 9. doi:10.3390/polym13162642

Nilsson, M., Miller, W., Cerviño, A., Bergmanson, J. P., & Brautaset, R. L. (2015). Evaluation of the anterior chamber angle in keratoconus and normal subjects. *Contact lens & anterior eye: the journal of the British Contact Lens Association*, *38*(4), 277–282.

Nishimura, T., & Takeichi, M. (2008). Shroom3-mediated recruitment of Rho kinases to the apical cell junctions regulates epithelial and neuroepithelial planar remodeling. *Development (Cambridge, England)*, *135*(8), 1493–1502.

Olivares Jiménez, J. L., Guerrero Jurado, J. C., Bermudez Rodriguez, F. J., & Serrano Laborda, D. (1997). Keratoconus: age of onset and natural history. *Optometry and vision science: official publication of the American Academy of Optometry*, *74*(3), 147–151.

Plageman, T. F., Jr, Chauhan, B. K., Yang, C., Jaudon, F., Shang, X., Zheng, Y., Lou, M., Debant, A., Hildebrand, J. D., & Lang, R. A. (2011a). A Trio-RhoA-Shroom3 pathway is required for apical constriction and epithelial invagination. *Development (Cambridge, England)*, *138*(23), 5177–5188.

Plageman, T. F., Jr, Zacharias, A. L., Gage, P. J., & Lang, R. A. (2011b). Shroom3 and a Pitx2-N-cadherin pathway function cooperatively to generate asymmetric cell shape changes during gut morphogenesis. *Developmental biology*, *357*(1), 227–234.

Ponting, C. P., Phillips, C., Davies, K. E., & Blake, D. J. (1997). PDZ domains: targeting signalling molecules to sub-membranous sites. *BioEssays: news and reviews in molecular, cellular and developmental biology*, *19*(6), 469–479.

Quantock, A. J., Winkler, M., Parfitt, G. J., Young, R. D., Brown, D. J., Boote, C., & Jester, J. V. (2015). From nano to macro: studying the hierarchical structure of the corneal extracellular matrix. *Experimental eye research*, *133*, 81–99.

Rabinowitz Y. S. (1998). Keratoconus. *Survey of ophthalmology*, *42*(4), 297–319.

Rabinowitz, Y. S., Galvis, V., Tello, A., Rueda, D., & García, J. D. (2021). Genetics vs chronic corneal mechanical trauma in the etiology of keratoconus. *Experimental eye research*, *202*, 108328.

Rabinowitz, Y. S., Maumenee, I. H., Lundergan, M. K., Puffenberger, E., Zhu, D., Antonarakis, S., & Francomano, C. A. (1992). Molecular genetic analysis in autosomal dominant keratoconus. *Cornea*, *11*(4), 302–308.

Radner Radner, W., Zehetmayer, M., Aufreiter, R., & Mallinger, R. (1998). Interlacing and cross-angle distribution of collagen lamellae in the human cornea. *Cornea*, *17*(5), 537–543.

Radner, W., & Mallinger, R. (2002). Interlacing of collagen lamellae in the midstroma of the human cornea. *Cornea*, *21*(6), 598–601.

Rebenitsch, R. L., Kymes, S. M., Walline, J. J., & Gordon, M. O. (2011). The lifetime economic burden of keratoconus: a decision analysis using a markov model. *American journal of ophthalmology*, *151*(5), 768–773.e2.

Regini, J. W., Elliott, G. F., & Hodson, S. A. (2004). The ordering of corneal collagen fibrils with increasing ionic strength. *Journal of molecular biology*, *336*(1), 179–186.

Reinstein, D. Z., Gobbe, M., Archer, T. J., Silverman, R. H., & Coleman, D. J. (2010). Epithelial, stromal, and total corneal thickness in keratoconus: three-dimensional display with artemis very-high frequency digital ultrasound. *Journal of refractive surgery (Thorofare, N.J.: 1995)*, *26*(4), 259–271.

Reprinted from "Layers of the Cornea", by BioRender.com (2020). Retrieved from https://app.biorender.com/biorender-templates

Ricard-Blum S. (2011). The collagen family. *Cold Spring Harbor perspectives in biology*, *3*(1), a004978.

Ryan, D. G., Oliveira-Fernandes, M., & Lavker, R. M. (2006). MicroRNAs of the mammalian eye display distinct and overlapping tissue specificity. *Molecular vision*, *12*, 1175–1184.

Shetty, R., Kaweri, L., Pahuja, N., Nagaraja, H., Wadia, K., Jayadev, C., Nuijts, R., & Arora, V. (2015). Current review and a simplified "five-point management algorithm" for keratoconus. *Indian journal of ophthalmology*, *63*(1), 46–53.

Smith, R. S., Korb, D., & John, S. W. (2002). A goniolens for clinical monitoring of the mouse iridocorneal angle and optic nerve. *Molecular vision*, *8*, 26–31.

Smolek, M. K., & Beekhuis, W. H. (1997). Collagen fibril orientation in the human corneal stroma and its implications in keratoconus. *Investigative ophthalmology & visual science*, *38*(7), 1289–1290.

Song, X., Stachon, T., Wang, J., Langenbucher, A., Seitz, B., & Szentmáry, N. (2015). Viability, apoptosis, proliferation, activation, and cytokine secretion of human keratoconus keratocytes after cross-linking. *BioMed research international*, *2015*, 254237.

Srinivas S. P. (2010). Dynamic regulation of barrier integrity of the corneal endothelium. *Optometry and vision science: official publication of the American Academy of Optometry*, *87*(4), E239–E254.

Sugar, J., & Macsai, M. S. (2012). What causes keratoconus? *Cornea*, *31*(6), 716–719.

Sykakis, E., Carley, F., Irion, L., Denton, J., & Hillarby, M. C. (2012). An in-depth analysis of histopathological characteristics found in keratoconus. *Pathology*, *44*(3), 234–239.

Tanaka, H., Murakami, Y., Ishii, I., & Nakata, S. (2009). Involvement of a forkhead transcription factor, FOXO1A, in UV-induced changes of collagen metabolism. *The journal of investigative dermatology. Symposium proceedings*, *14*(1), 60–62. https://doi.org/10.1038/jidsymp.2009.2

Tariq, M., Belmont, J. W., Lalani, S., Smolarek, T., & Ware, S. M. (2011). SHROOM3 is a novel candidate for heterotaxy identified by whole exome sequencing. *Genome biology*, *12*(9), R91.

Torricelli, A. A., & Wilson, S. E. (2014). Cellular and extracellular matrix modulation of corneal stromal opacity. *Experimental eye research*, *129*, 151–160.

Torricelli, A. A., Singh, V., Santhiago, M. R., & Wilson, S. E. (2013). The corneal epithelial basement membrane: structure, function, and disease. *Investigative ophthalmology & visual science*, *54*(9), 6390–6400.

Trattler, W. B., Majmudar, P. A., Luchs, J. I., Swartz, T. S. (2010). Cornea Handbook. SLACK Incorporated; 2010.

Tsunoda, S., Sierralta, J., Sun, Y., Bodner, R., Suzuki, E., Becker, A., Socolich, M., & Zuker, C. S. (1997). A multivalent PDZ-domain protein assembles signalling complexes in a G-protein-coupled cascade. *Nature*, *388*(6639), 243–249.

Wagner, H., Barr, J. T., & Zadnik, K. (2007). Collaborative Longitudinal Evaluation of Keratoconus (CLEK) Study: methods and findings to date. *Contact lens & anterior eye: the journal of the British Contact Lens Association*, *30*(4), 223–232.

Wheeler, J., Hauser, M. A., Afshari, N. A., Allingham, R. R., & Liu, Y. (2012). The Genetics of Keratoconus: A Review. *Reproductive system & sexual disorders: current research*, (Suppl 6), 001.

Wilson S. E. (2020). Bowman's layer in the cornea- structure and function and regeneration. *Experimental eye research*, *195*, 108033.

Wong, H. C., Bourdelas, A., Krauss, A., Lee, H. J., Shao, Y., Wu, D., Mlodzik, M., Shi, D. L., & Zheng, J. (2003). Direct binding of the PDZ domain of Dishevelled to a conserved internal sequence in the C-terminal region of Frizzled. *Molecular cell*, *12*(5), 1251–1260.

Yi, X., Wang, Y., & Yu, F. S. (2000). Corneal epithelial tight junctions and their response to lipopolysaccharide challenge. *Investigative ophthalmology & visual science*, *41*(13), 4093–4100. Parker, J., Dockery, P., Preda-Naumescu, A., Jager, M., van Dijk, K., Dapena, I., & Melles, G. (2021). Descemet Membrane Endothelial Keratoplasty and Bowman Layer Transplantation: An Anatomic Review and Historical Survey. *Ophthalmic research*, *64*(4), 532–553.

Young, R. D., Swamynathan, S. K., Boote, C., Mann, M., Quantock, A. J., Piatigorsky, J., Funderburgh, J. L., & Meek, K. M. (2009). Stromal edema in klf4 conditional null mouse cornea is associated with altered collagen fibril organization and reduced proteoglycans. *Investigative ophthalmology & visual science*, *50*(9), 4155–4161.